Electronic Supplementary Information

Ruthenium or Osmium? On the Role of the Metal in Carbonylchlorido Complexes for Photodynamic Therapy

Gina Elena Giacomazzo,[a] Fortuna Ponte,[b] Valentina Ceccherini,[a] Lorenzo Gianassi,[a] Gloria Mulas,[c] Emilia Sicilia,[b] Francesca Cencetti,[c] Barbara Valtancoli,[a] Luca Conti[a] and Claudia Giorgi[a]

[a.] Department of Chemistry "*Ugo Schiff*", University of Florence, Via della Lastruccia 3, 50019, Sesto Fiorentino (FI), Italy.
[b.] Department of Chemistry and Chemical Technologies University of Calabria, via Pietro Bucci, 87036 Arcavacata Rende, Cs, Italy.
[c.] Department of Experimental and Clinical Biomedical Sciences "*Mario Serio*", University of Florence, Viale Morgagni 50, Florence 50134, Italy.

List of Contents

1. *Synthesis and characterization*
2. *Determination of $^1O_2$ quantum yields*
3. *Determination of luminescence quantum yields*
4. *Chemical stability and photoreactivity of metal complexes*
5. *DFT calculations*
    1. ***2a*** *and* ***2b*** *precursors*
    2. ***RuCOCl*** *and* ***OsCOCl*** *complexes*
    3. *Computational details*
6. *Biological studies*
    1. *Cell culture and treatments*
    2. *Cellular uptake*
    3. *Cell viability assay*

1. Synthesis and characterization

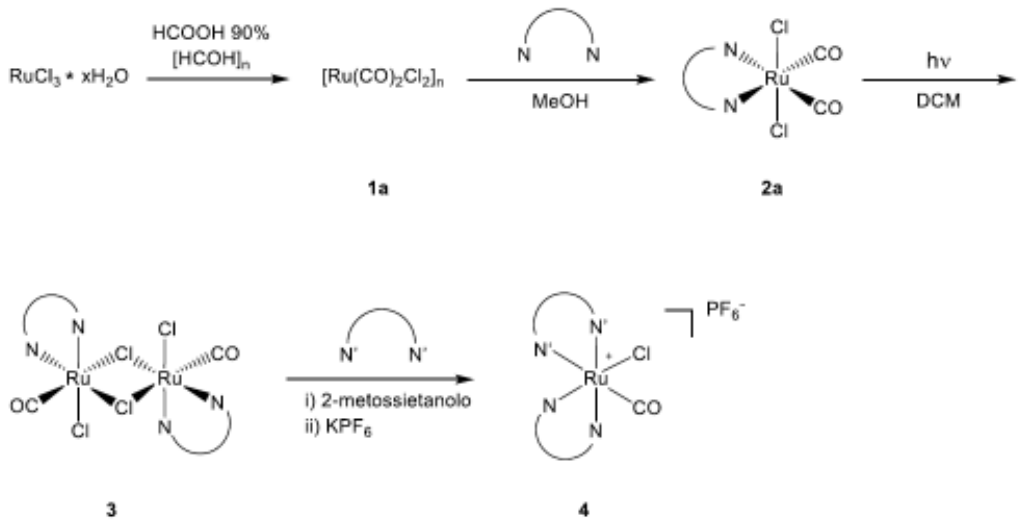

Scheme S1. Schematization of the general reaction pathway for the obtaining of Ru(II)-based heteroleptic carbonylchlorido complexes $[Ru(NN)(N'N')COCl]^+$.

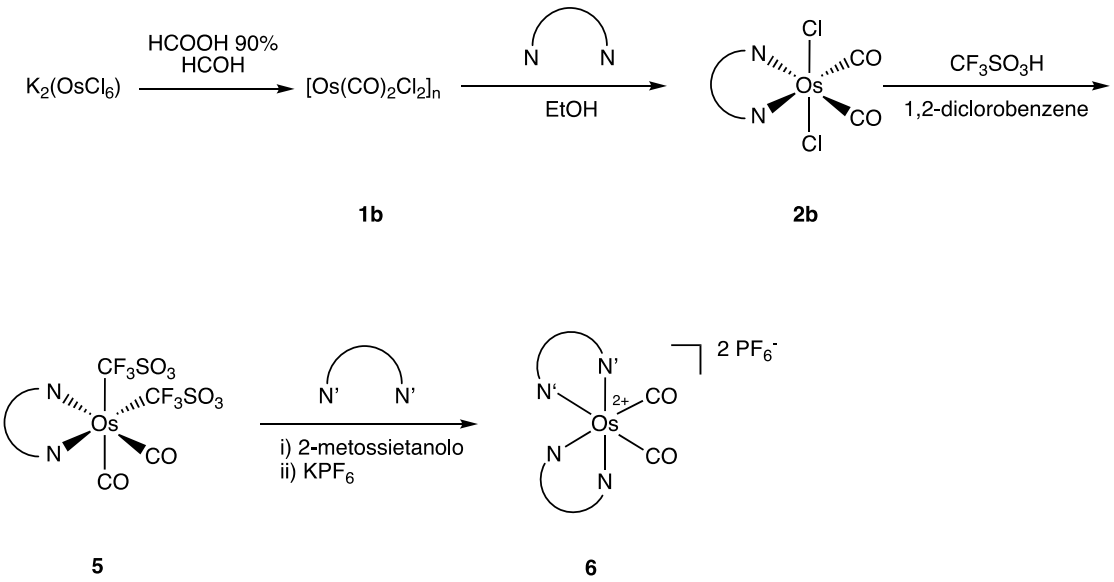

Scheme S2. Schematization of the general reaction pathway for the obtaining of Os(II)-based heteroleptic carbonyl complexes $[Os(NN)(N'N')(CO)_2]^+$.

Synthesis of $[Ru(CO)_2Cl_2]_n$ (1a) and $[Os(CO)_2Cl_2]_n$ (1b)

$RuCl_3 \cdot 3H_2O$ (500 mg, 2.41 mmol) was dissolved in 90% HCOOH (16 mL, 0.15 M) under N_2 atmosphere and paraformaldehyde ($[HCOH]_n$ 316.5 mg, 10.54 mmol) was added. The mixture was heated to reflux under a constant flow of nitrogen and protected from light. Over the course of six hours, the reaction mixture changed colour from green to blue and finally to a clear yellow solution. The excess of formic acid was then removed under reduced pressure, affording a yellow-orange glassy solid. The solid was triturated with hexane, filtered, and dried over vacuum to yield compound **1a** as a yellow solid (380 mg, yield 68%).

Similarly, K_2OsCl_6 (100 mg, 0.2 mmol) was dissolved in 90% HCOOH (4 mL, 0.05 M) in a screw-cap reaction vial under N_2 atmosphere and paraformaldehyde ($[HCOH]_n$ 60 mg, 2.0 mmol) was added. The mixture was heated to reflux under N_2 and protected from light until a clear yellow solution was obtained. The excess of formic acid was removed under reduced pressure, affording an orange solid. The residue was dissolved in acetone, filtered to remove KCl, and concentrated under reduced pressure. The resulting solid was triturated with hexane, filtered, and dried under vacuum to yield compound **1b** as an orange solid (63 mg, quantitative yield).

Both the polymeric precursors were used in the next reaction steps without further purification.

Synthesis of [Ru(Me_2bpy)(CO)$_2$Cl$_2$] (2a)
The polymeric precursor 1a (100 mg, 0.43 mmol) was dissolved in 6.5 mL of anhydrous methanol under N_2 atmosphere and Me_2bpy (72.2 mg, 0.392 mmol) was added. The reaction mixture was heated to reflux while protected from light. After 1 h 30 min, a yellow product precipitated, which was hot filtered, washed with methanol and dried under vacuum. The product was obtained as a yellow solid (127 mg, 78% yield).
The spectroscopic data are in good agreement with those reported in the literature. [1]

^{1}H-NMR (400 MHz; $(CD_3)_2SO$): δ 9.02 (d, J=5.6 Hz, 2H, H2), 8.64 (s, 2H, H5), 7.66 (d, J=5.6 Hz, 2H, H3); 2.59 (s, 6H, CH_3) ppm.
^{13}C-NMR (100 MHz, $(CD_3)_2SO$): δ 197.2, 155.2, 153.6, 153.4, 129.5, 125.7, 21.9 ppm.

Synthesis of [Os(Me_2bpy)(CO)$_2$Cl$_2$] (2b)
The polymeric precursor **1b** (32 mg, 0.1 mmol) and Me_2bpy (15.5 mg, 0.08 mmol) were suspended in deoxygenated ethanol (1.6 mL, 0.06 M) in a screw-cap reaction vial under N_2 atmosphere. The reaction mixture was heated to 90 °C while protected from light. After 5 h, a brick-red suspension formed, which was filtered and washed with ethanol to afford a yellow-ochre solid (28 mg, 56% yield).

^{1}H-NMR (400 MHz; $(CD_3)_2SO$): δ 8.95 (d, J=4.4 Hz, 2H, H2), 8.72 (s, 2H, H5), 7.69 (d, J=4.8 Hz, 2H, H3); 2.63 (s, 6H, CH_3) ppm.
^{13}C-NMR (100 MHz; $(CD_3)_2SO$): attempts to record the spectrum were unsuccessful because of insufficient solubility.

Synthesis of [Ru(Me_2bpy)(dppn)(CO)Cl]PF_6 (RuCOCl)
To a suspension of **2a** (50 mg, 0.12 mmol) in degassed 2-methoxyethanol (6 mL, 0.02 M) were added dppn (40.2 mg, 0.121 mmol) and TMAO (17.8 mg, 0.13 mmol). The reaction mixture was heated at reflux under N_2 atmosphere and protected from light. After 3 hours, a dark-reddish solution was obtained, and the addition of aqueous KPF_6 (0.1 M) led to the precipitation of the product as its hexafluorophosphate salt. The complex was collected by vacuum filtration, washed with water and diethyl ether. The crude product was purified by flash chromatography on neutral alumina (activated at 5%) using a dichloromethane/ethyl acetate gradient (15:1 to 5:1) as the eluent, affording **RuCOCl** as an ochre-yellow solid (54 mg, 54% yield).

^{1}H-NMR (400 MHz; $(CD_3)OD$): δ 10.03 (d, 1H, J=8 Hz, trans-Cl), 9.91 (d, 1H, J=7.6 Hz, trans-CO), 9.88 (d, 1H, J=4 Hz, trans-Cl), 9.84-9.78 (m, 2H, trans-Cl/CO), 9.74 (d, 1H, J=8 Hz, trans-Cl), 9.49 (d, 1H, J=5.6 Hz, trans-CO), 9.32 (d, 1H, J=5.6 Hz, trans-Cl), 9.18 (s, 1H, trans-Cl), 9.14 (s, 1H, trans-CO), 9,12 (s, 1H, trans-Cl) 9.09 (s, 1H, trans-CO), 8.66-8.60 (m, 2H, trans-Cl/CO), 8.52 (s, 1H, trans-Cl), 8.47 (s, 1H, trans-CO), 8.41-8.25 (m, 6H, trans-Cl/CO), 8.15 (d, 1H, J=5.2 Hz, trans-Cl), 8,02-7.94 (m, 3H, trans-Cl/CO), 7.86-7.82 (m, 2H, trans-Cl/CO), 7.77-7.70 (m, 4H, trans-Cl/CO), 7,68 (d, 1H, J=6 Hz, trans-CO), 7.44 (d, 1H, J=6 Hz, trans-Cl), 7.18 (d, 1H, J=5.6 Hz, trans-Cl), 7.12 (d, 1H, J=6 Hz, trans-CO), 2.79 (s, 3H, trans-CO), 2.75 (s, 3H, trans-Cl), 2.48 (s, 3H, trans-Cl), 2.46 (s, 3H, trans-CO).

^{1}H-NMR analysis (**Fig. S3**) is consistent with a 62% *trans*-CO and 38% *trans*-Cl isomeric mixture, according to literature. [2] The relative abundance being determined by integration of proton signals in CD_3OD. The spectrum shows two distinct sets of signals, one for each isomer, comprising 18 aromatic resonances (12 from dppn and 6 from Me_2bpy) and two aliphatic signals from Me_2bpy methyl groups. Individual signal assignment was complicated by the large number of signals and by their partial overlapping.

^{13}C-NMR (100 MHz; $(CD_3)OD$): attempts to record the spectrum were unsuccessful because of insufficient solubility.
HR-MS: (ESI+) m/z: calcd. for $C_{35}H_{24}ON_6ClRu$ $[M\text{-}PF_6]^+$ 681.0644, measured: 681.07566.

Synthesis of [Os(Me_2bpy)(dppn)(CO)Cl]PF_6 (OsCOCl)
To a suspension of **2b** (50 mg, 0.10 mmol) in 5 mL of degassed 2-methoxyethanol were added dppn (33.10 mg, 0.10 mmol) and TMAO (16.71 mg, 0.150 mmol). The reaction mixture was heated at reflux under N_2 atmosphere

and protected from light. After 1 h a dark-red solution was obtained. Addition of aqueous KPF_6 (0.1 M) led to the precipitation of the product, which was collected by vacuum filtration and washed with water and diethyl ether. The crude product was dissolved in dichloromethane, washed with water (3 x 10 mL), brine (1 x 10 mL), dried over Na_2SO_4 and concentrated under reduced pressure.
The product was purified by flash chromatography on silica gel, using dichloromethane/methanol (gradient from 60:1 to 50:1) as eluent, affording **OsCOCl** as a red solid (30 mg, 32% yield).

^{1}H-NMR 400 MHz; $(CD_3)_2CO$): δ 10.14 (d, 1H, J=4.4 Hz, trans-Cl), 9.96 (d, 1H, J=7.2 Hz, trans-Cl), 9.87 (d, 1H, J=4.8 Hz, trans-CO), 9.76 (d, 1H, J=5.6 Hz, trans-Cl), 9.71 (dd, 1H, J_1=7.6 Hz, J_2=1.6 Hz, trans-CO), 9.69-9.65 (m, 2H), 9.39 (d, 1H, J= 6 Hz, trans-Cl), 9.21 (s, 1H, trans-Cl), 9.14 (s, 1H, trans-CO), 9.13 (s, 1H, trans-Cl), 9.07 (s, 1H, trans-CO), 8.79 (bs, 1H, trans-CO), 8.71-8.70 (m, 2H, trans-Cl/CO), 8.64-8.60 (m, 2H, trans-Cl/CO), 8.52 (dd, 1H, J_1=13.6 Hz, J_2=2.8 Hz, trans-Cl), 8.44-8.35 (m, 4H, trans-Cl/CO), 8.31 (dd, 1H, J_1=13.6 Hz, J_2=2.8 Hz, trans-CO), 8.15 (d, 1H, J=6 Hz, trans-CO), 8.05-8.00 (m, 2H, trans-Cl/CO), 7.96-7.92 (m, 2H, trans-Cl/CO) , 7.80-7.74 (m, 5H, trans-Cl/CO), 7.41 (d, 1H, J=5.6 Hz, trans-Cl), 7.17 (t, 2H, J=6.8 Hz, trans-CO), 2.83 (s, 3H, trans-CO), 2,82 (s, 3H, trans-Cl), 2,50(s, 3H, trans-Cl), 2,48 (s, 3H, trans-CO).

^{1}H-NMR analysis (**Fig. S5**) is consistent with a 53% *trans*-CO and 47% *trans*-Cl isomeric mixture, accordingly to literature.[2] The relative abundance being determined by integration of proton signals in $(CD_3)_2CO$. The spectrum shows two distinct sets of signals, one for each isomer, comprising 18 aromatic resonances (12 from dppn and 6 from Me_2bpy) and two aliphatic signals from Me_2bpy methyl groups. Individual signal assignment was complicated by the large number of signals and by their partial overlapping.

^{13}C-NMR (100 MHz; $(CD_3)_2CO$): δ 178.1, 178.0, 160.0, 159.7, 157.3, 156.8, 156.4, 155.7, 155.6, 155.4, 155.3, 153.6, 153.6, 153.5, 153.1, 152.5, 151.3, 150.8, 150.7, 150.0, 147.7, 139.1, 136.8, 136.8, 135.9, 135.9, 135.7, 135.3, 133.9, 129.8, 129.5, 129.3, 129.2, 129.1, 128.9, 128.7, 128.6, 128.4, 127.9, 126.0, 125.9, 125.8, 124.9, 21.3, 20.9, 20.8, 20.7 ppm.

HR-MS: (ESI+) m/z: calcd. for $C_{35}H_{24}ON_6ClOs$ $[M\text{-}PF_6]^+$ 771.1300, measured: 771.13319.

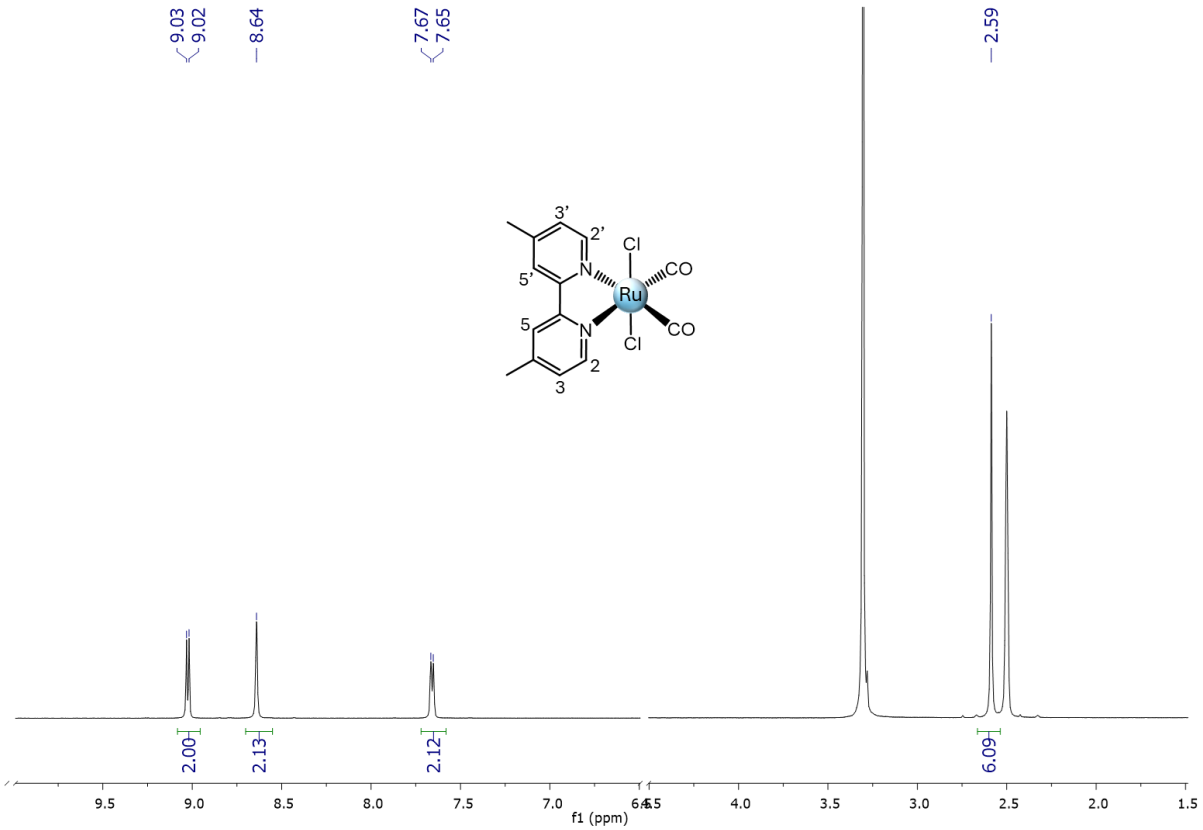

Figure S1. ^{1}H-NMR (400 MHz) of [Ru(Me$_2$bpy)(CO)$_2$Cl$_2$] (**2a**) in (CD$_3$)$_3$SO.

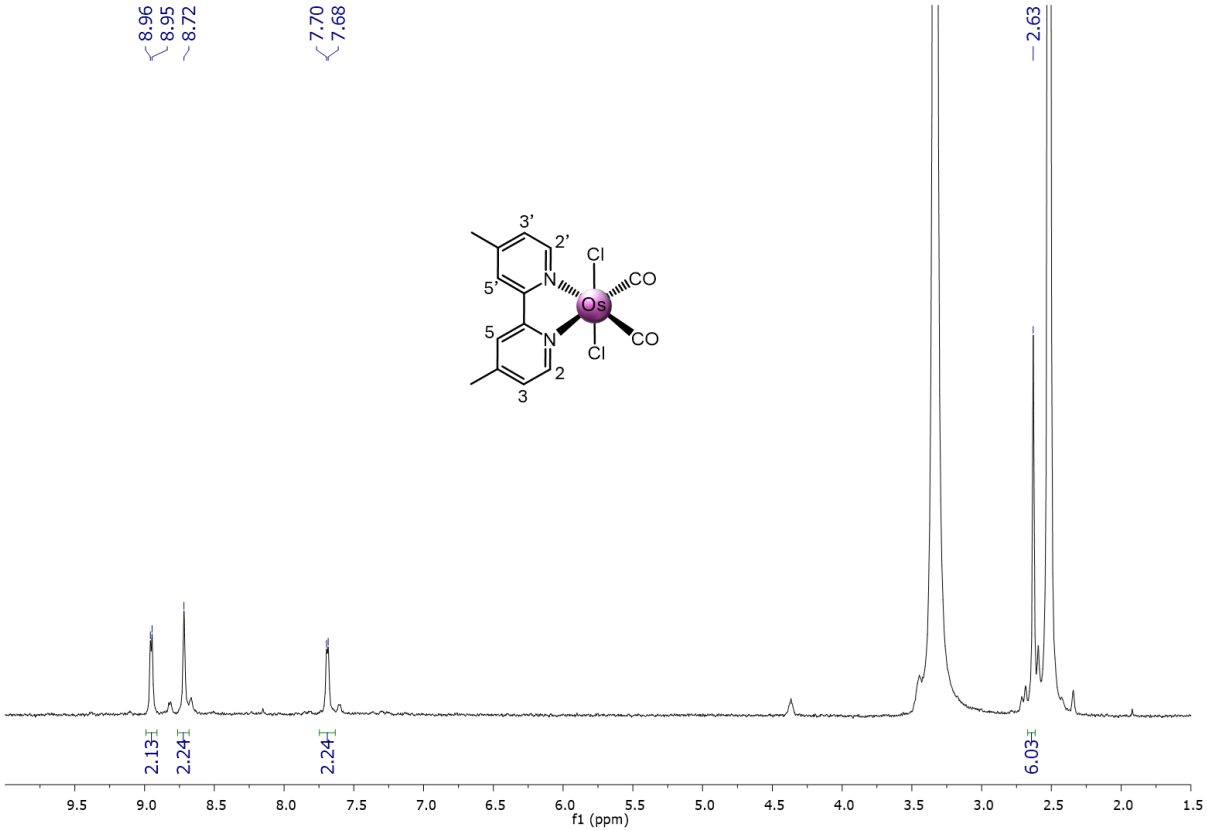

Figure S2. ^{1}H-NMR (400 MHz) of [Os(Me$_2$bpy)(CO)$_2$Cl$_2$] (**2b**) in (CD$_3$)$_3$SO.

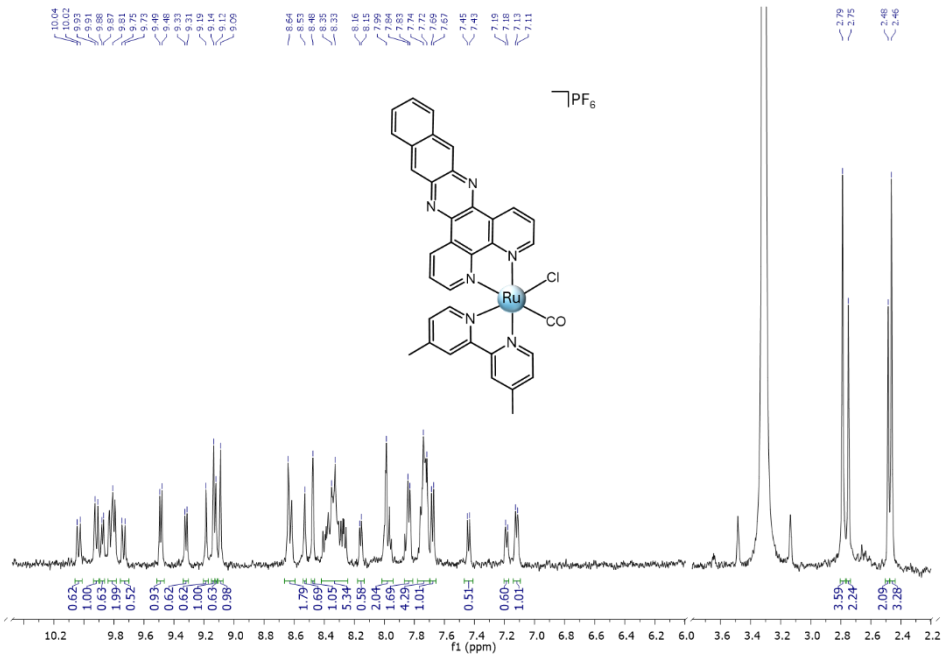

Figure S3. ^{1}H-NMR (400 MHz) of [Ru(Me$_2$bpy)(dppn)(CO)Cl]PF$_6$ (**RuCOCl**) in CD$_3$OD.

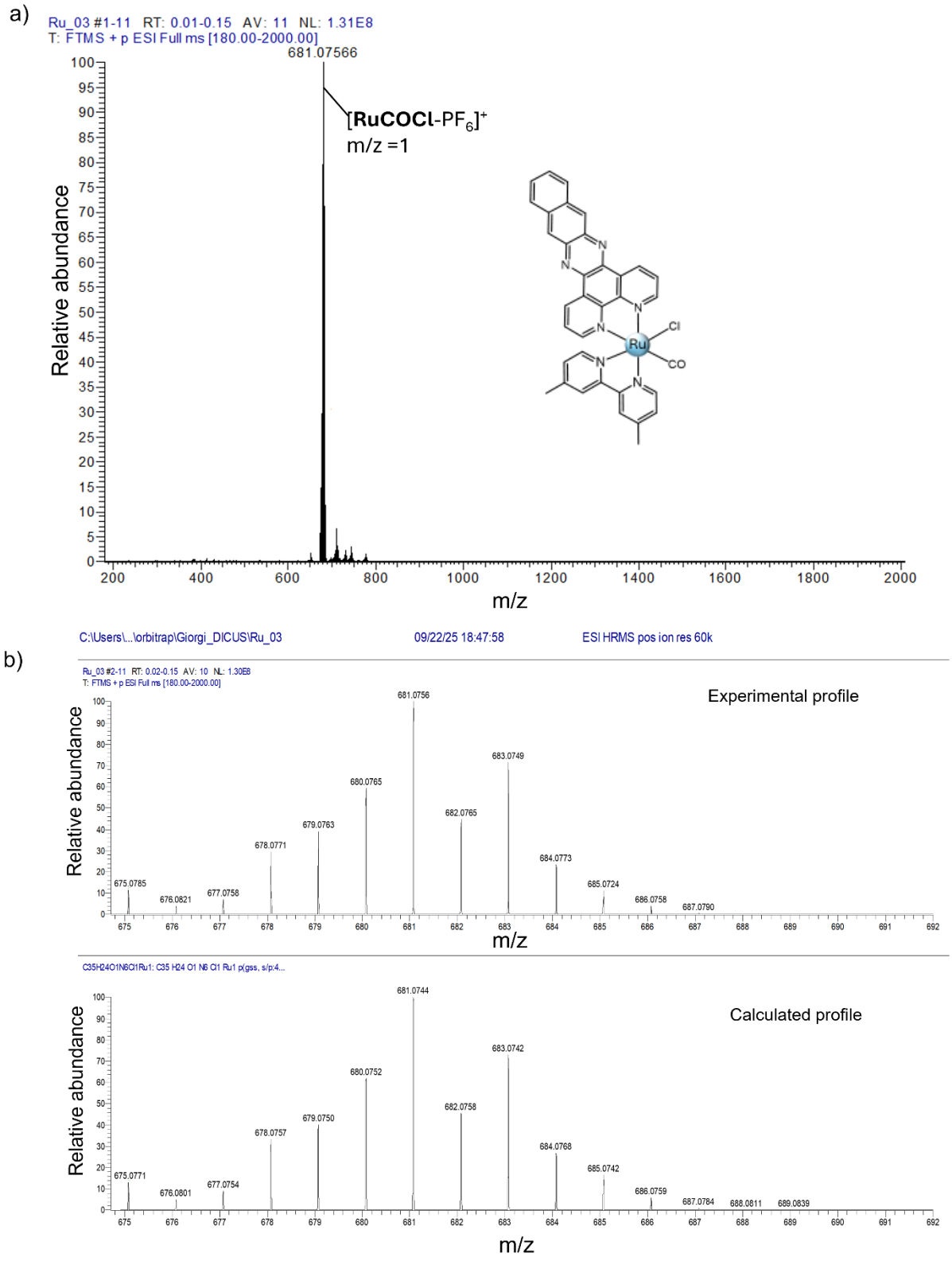

Figure S4. HR ESI-MS spectrum of [Ru(Me_2bpy)(dppn)(CO)Cl]PF_6 (**RuCOCl**) (a) along with the comparison between the measured and calculated isotopic pattern for [**RuCOCl** -PF_6]$^+$ (z = 1) ion (b).

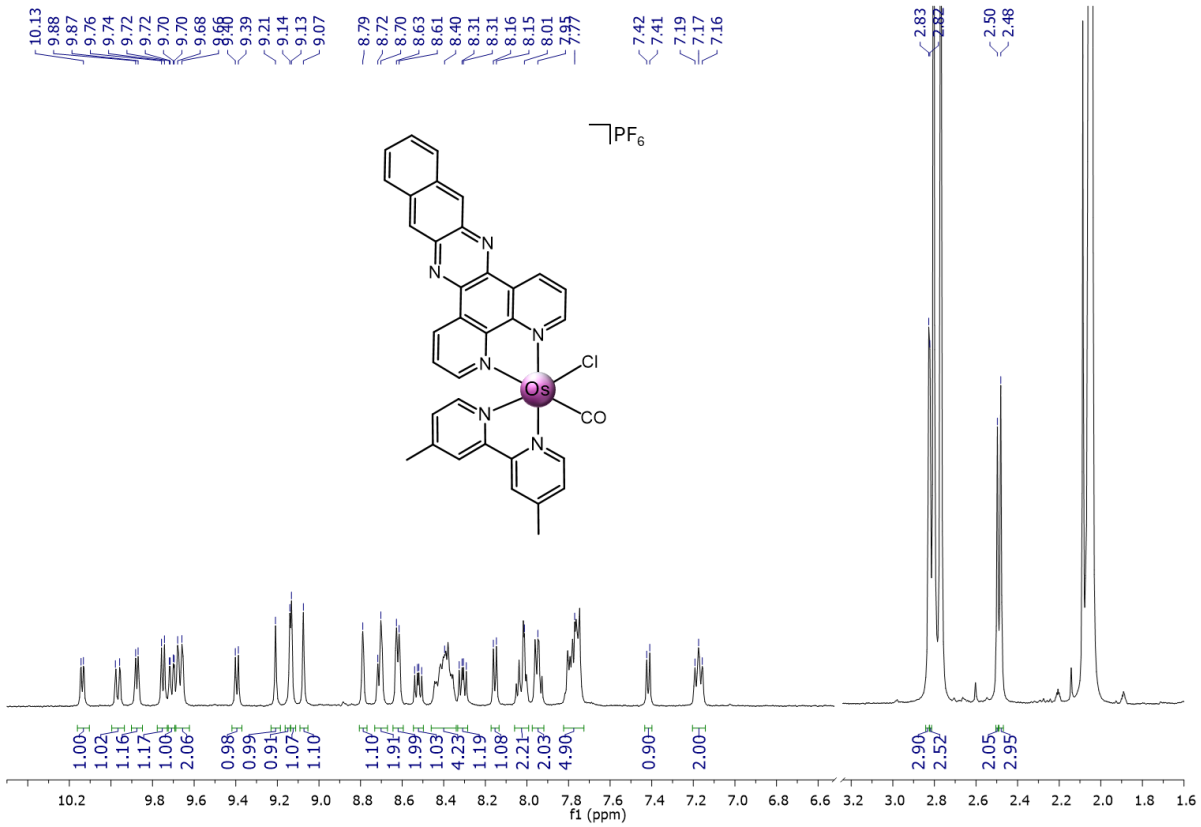

Figure S5. ^{1}H-NMR (400 MHz) of [Os(Me_2bpy)(dppn)(CO)Cl]PF_6 (**OsCOCl**) in $(CD_3)_2CO$.

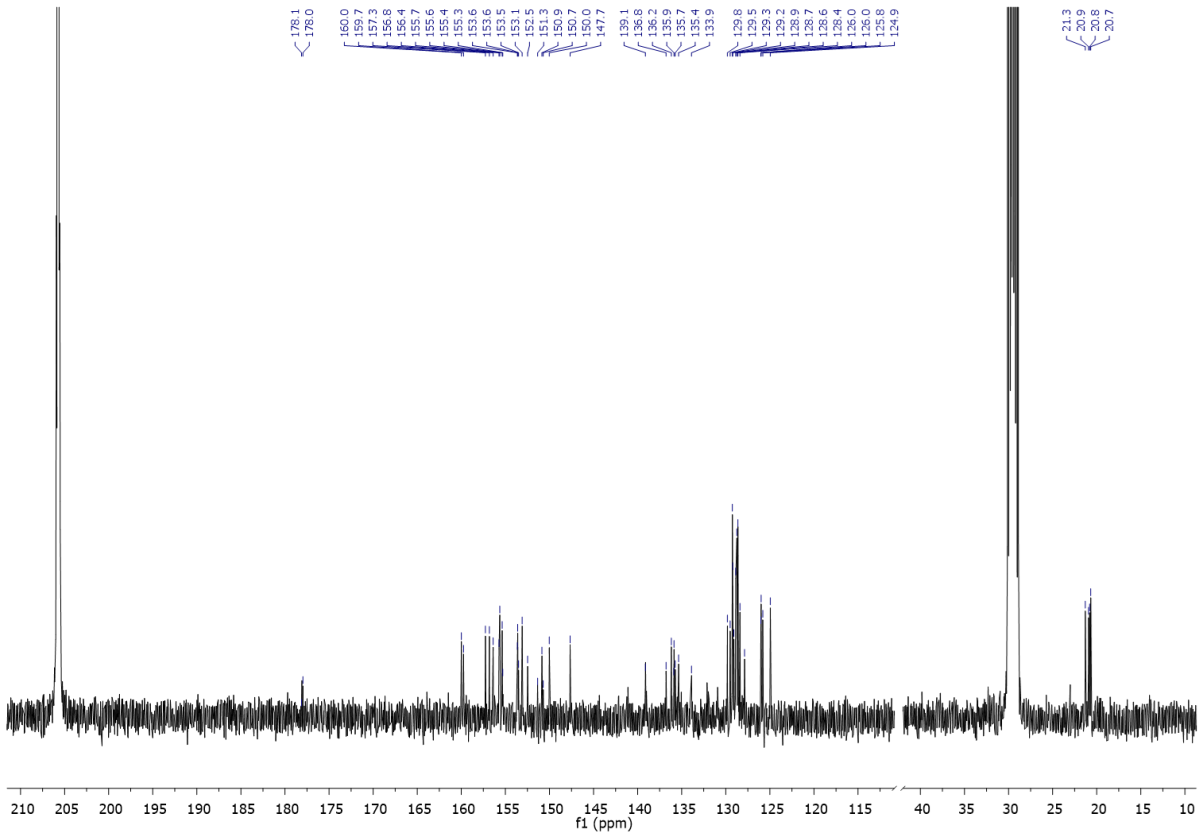

Figure S6. ^{13}C-NMR (400 MHz) of [Os(Me_2bpy)(dppn)(CO)Cl]PF_6 (**OsCOCl**) in $(CD_3)_2CO$.

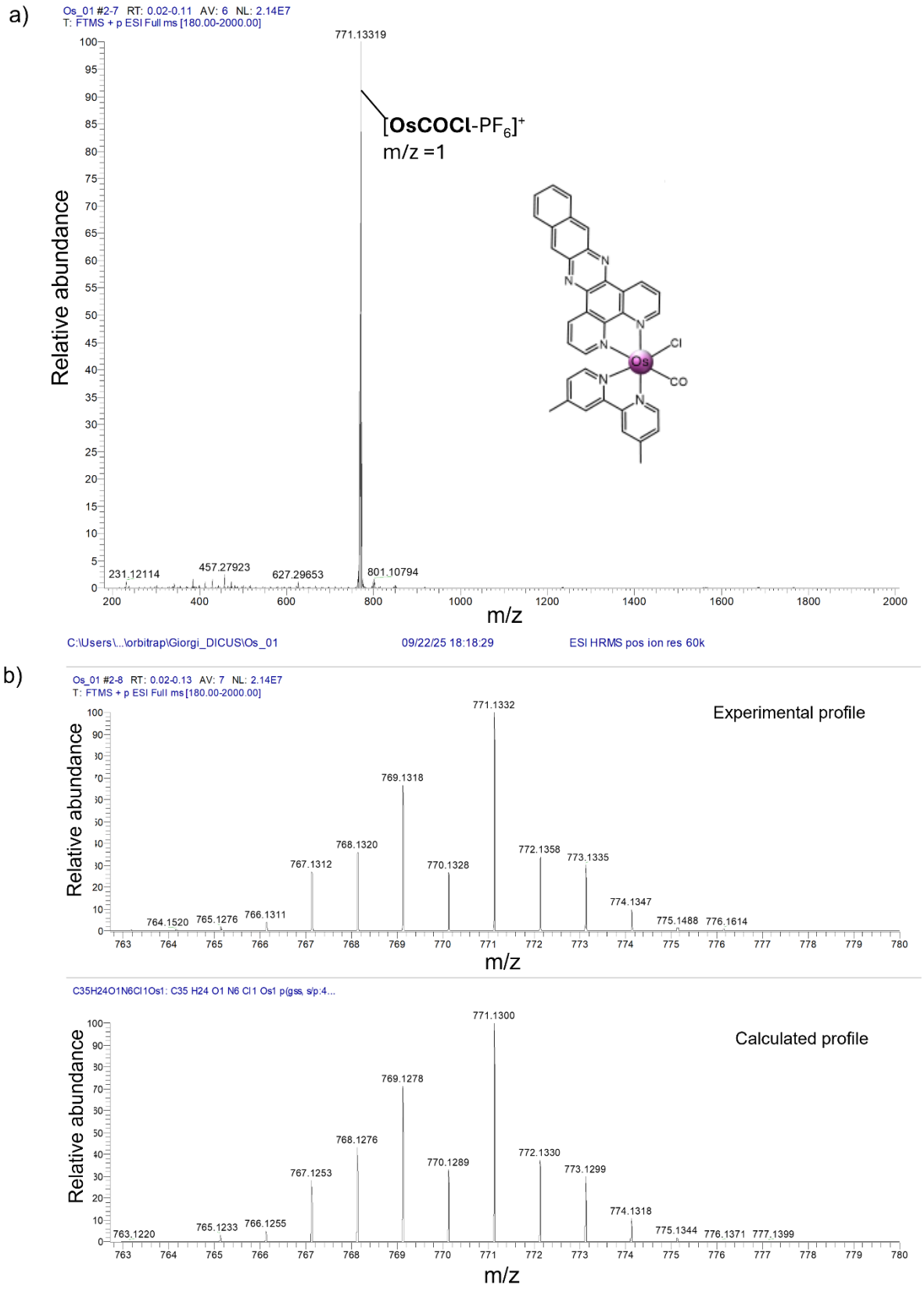

Figure S7. HR ESI-MS spectrum of [Os(Me_2bpy)(dppn)(CO)Cl]PF_6 (**OsCOCl**) (a) along with the comparison between the measured and calculated isotopic pattern for [**OsCOCl** -PF_6]$^+$ (z = 1) ion (b).

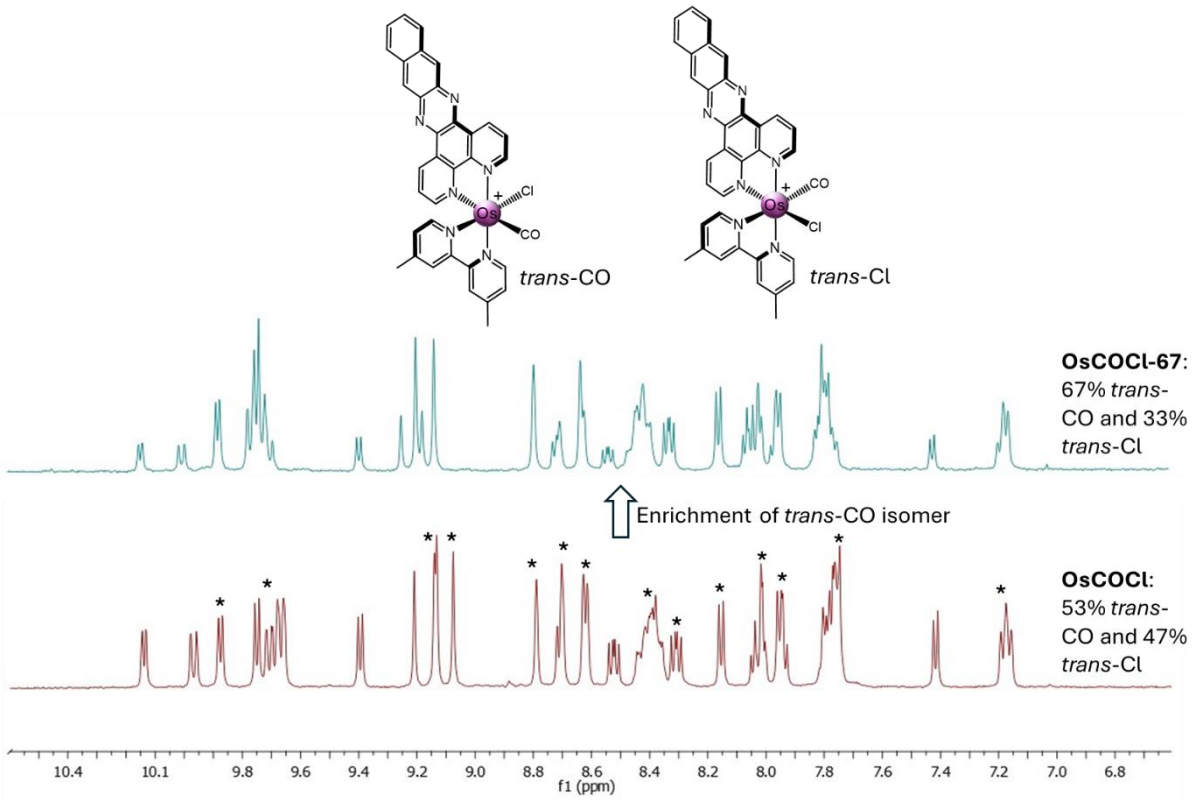

Figure S8. Comparison among ^{1}H-NMR (400 MHz) spectra of **OsCOCl** (53% *trans*-CO, 47% *trans*-Cl, bottom) and **OsCOCl67** (67% *trans*-CO, 33% *trans*-Cl, top) in $(CD_3)_2CO$.

Electronic Absorption, Fluorescence and NMR Measurements

Electronic absorption spectra of compounds were acquired by using a PerkinElmer Lambda 6 spectrophotometer in a 1x1 cm quartz cuvette. Fluorescence characterization of complexes and measurements of the phosphorescence signal of $^1O_2$ were carried out on a Horiba FluoroMax Plus spectrofluorometer, in the latter case the instrument was also equipped with a long-pass filter at 850 nm.

2. Determination of $^1O_2$ quantum yields

The quantum yields of $^1O_2$ generation (ϕ_Δ) by complexes of this study were analysed through the direct measurement of $O_2(^1\Delta_g) \rightarrow {}^3O_2$ phosphorescence signal at 1270 nm, upon excitation (λ_{exc} = 440 nm) in air-saturated acetonitrile solutions. Experiments were run on solutions of complexes at increasing concentrations (2-12 μM), with their MLCT absorbances within the range 0.02 - 0.2. Phosphorescence signals were filtered by a low-cutoff filter at 850 nm and collected by a N_2 cooled InGaAs photodiode with an integration time of 1 second.
ϕ_Δ values were obtained as previously described[3,4] by using the following equation:

$$\Phi_\Delta = \Phi_{ref} \frac{m_x}{m_{ref}}$$

where ϕ_{ref} is the quantum yield of the standard photosensitizer $[Ru(phen)_3]Cl_2$ (ϕ_{ref} = 0.38 ± 0.06),[5] m_x and m_{ref} are the experimental determined slopes of the linear fits between the integrated area of the phosphorescence signals (1225-1325 nm range) and the absorption factors ($1-10^{-Abs}$) at 440 nm for the investigated complexes and the reference compound.

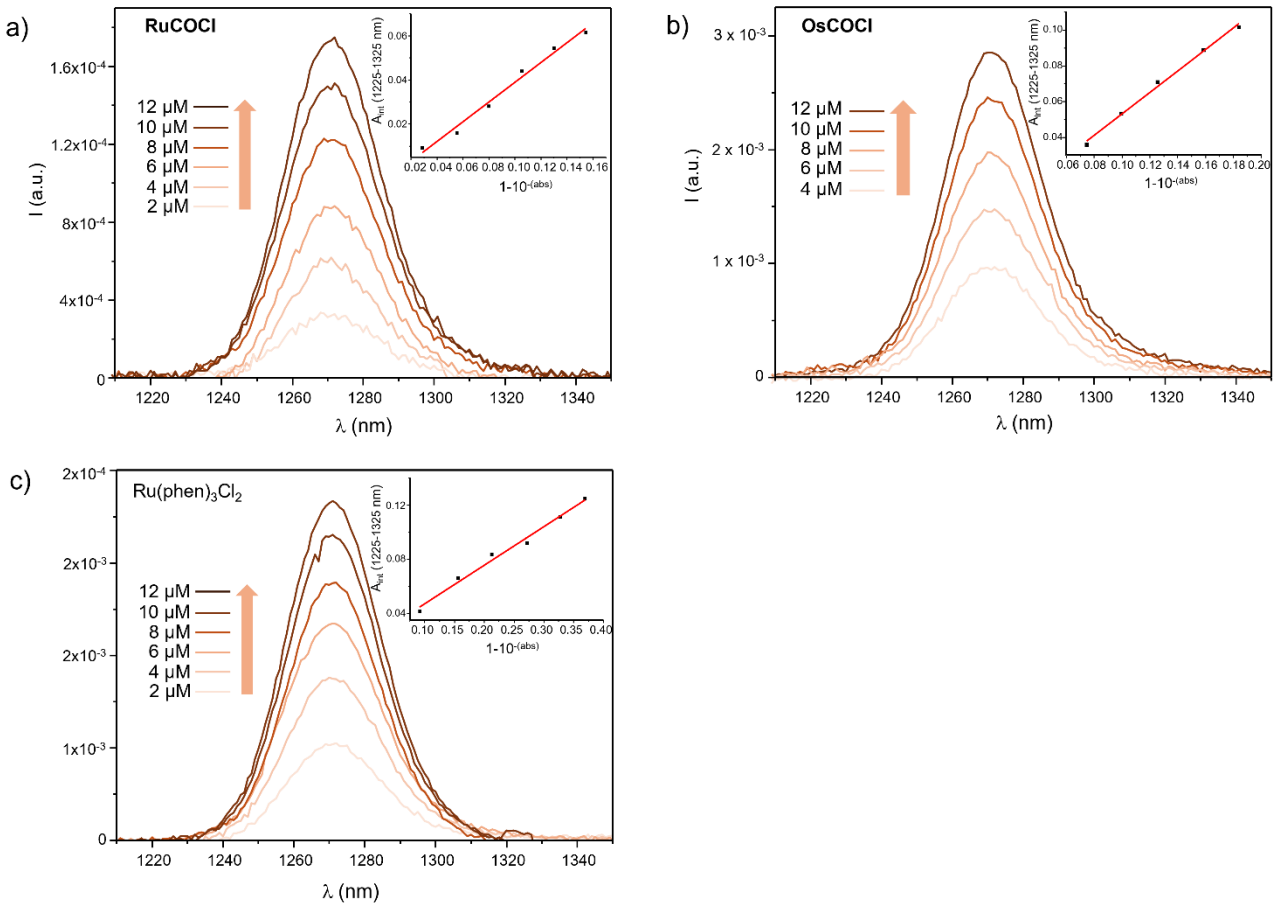

Figure S9. Determination of the $^1O_2$ quantum yields of **RuCOCl** (a), **OsCOCl** (b) and $Ru(phen)_3Cl_2$ as reference standard (c) by direct measurement of the $^1O_2$ phosphorescence. Insets on top right of each graph show the linear fittings between the integrated areas of the emission signals collected at various complexes' concentrations (A_{int}) and their correspondent absorption factors ($1-10^{-Abs}$) ([Ru/Os] = 2-12 μM, λ_{exc} 440 nm).

3. Determination of Luminescence Quantum Yield

The luminescence quantum yields (ϕ_L) of **RuCOCl** and **OsCOCl** were determined in acetonitrile and water, under both aerated and degassed conditions, by recording the emission spectra (λ_{ex} = 442 nm) of a series of solutions with the ^{1}MLCT absorbance values in the 0.08-0.02 range, using a 1 cm optical-path-length quartz cuvette. Measurements were performed on a Horiba FluoroMax Plus spectrophotometer.

For each solution, the integrated emission was plotted as a function of the absorbed light fraction ($1-10^{-abs}$) at the excitation wavelength. The slope of the resulting linear regression, which is proportional to the luminescence quantum yield of the sample ($\phi_{L\,(PS)}$), was used to calculate $\phi_{L\,(PS)}$ according to the following equation:

$$\phi_{L\,(PS)} = \phi_{ST}\frac{slope_{PS}}{slope_{ST}}\left(\frac{\eta_{PS}}{\eta_{ST}}\right)^2$$

where ϕ_{ST} is the luminescence quantum yield of the reference standard $[Ru(phen)_3]Cl_2$ for which the reported values are 0.028 in acetonitrile and 0.058 in water.[6] The refractive index ratio $\left(\frac{\eta_{PS}}{\eta_{ST}}\right)^2$ is equal to unity, as both the samples and the standard were measured in the same solvent.

The obtained quantum yields, reported in Table S1, indicate generally weak emission from both complexes, with acetonitrile solutions of **OsCOCl** exhibiting the highest values, with nearly identical ϕ_L under aerated and degassed conditions of respectively 0.0156(6) and 0.0151(5).
In aqueous media, the luminescence of **OsCOCl** is strongly reduced compared to acetonitrile solutions, by approximately 18-fold, whereas **RuCOCl** displayed a higher ϕ_L (ϕ_L 0.0043(2) in aerated water, roughly twice than in aerated acetonitrile). This different solvent-dependent behavior might be tentatively explained with a stronger stabilization of non-radiative deactivation pathways for the Os(II) complex in water, potentially associated with enhanced spin-orbit coupling effects and solvent-mediated quenching, which more effectively suppress emission relative to the Ru(II) analogue.

	ϕ_L CH_3CN	ϕ_L H_2O
RuCOCl	0.00224(9)	0.0043(2)
	0.00139(7)[a]	-
OsCOCl	0.0156(6)	0.00087(6)
	0.0151(5) [a]	-

Table S1: Luminescence quantum yields (ϕ_L) in acetonitrile and water. [a] Measured under degassed conditions.

4. Chemical Stability and Photoreactivity of Metal Complexes

Prior to the evaluation of the biological activity of the two complexes, their chemical stability in aqueous medium were investigated.
To this aim, the electronic absorption spectra of 10 µM solutions of both complexes in phosphate buffered saline (PBS, pH = 7.4) under dark and over a total time of 24 hours were registered; the results are reported in Figure S10.

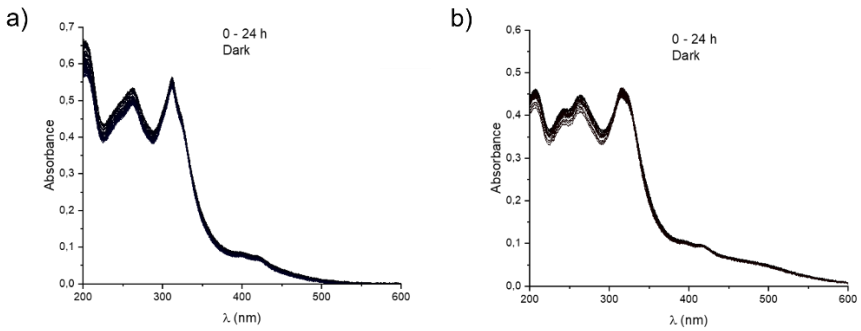

Figure S10: Electronic absorption spectra of 10 µM solutions of **RuCOCl** (a) and **OsCOCl** (b) in phosphate buffered saline PBS (pH=7.4), collected at increasing incubation times under dark conditions over a total period of 24 h.

As shown, the absorption profiles of the two metal complexes did not undergo appreciable variations during the interval of time tested, denoting a remarkable stability under these conditions.
The exposure to prolonged LED irradiation in aqueous solutions was also investigated. This, analogously to stability measurements, was carried out by recording the UV-Vis spectra of 10 µM aqueous solutions of the two complexes subjected to increasing irradiation times (λ_{max} 462 nm, 160 mW) with LED light. Irradiation times of up to 1 hour were explored, well beyond the total irradiation time of 15 min employed in the biological assays (*vide infra*), in order to assess whether prolonged photoactivation could induce changes in the absorption profile, particularly in the MLCT region, since variations in this spectral domain may indicate rearrangements around the metal center and, consequently, the occurrence of possible photodissociation processes at longer irradiation times. The results obtained in PBS media are reported below.

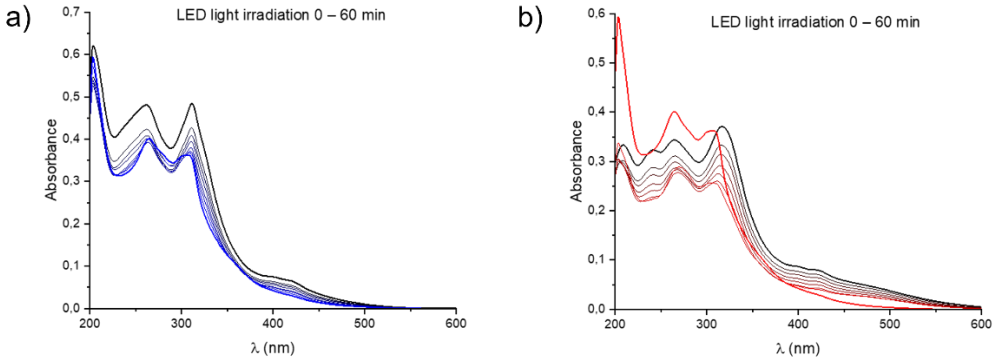

Figure S11: Electronic absorption spectra of 10 μM solutions of **RuCOCl** (a) and **OsCOCl** (b) the PSs in phosphate buffered saline (pH=7.4) exposed to increasing LED light (160 mW) irradiation times, up to 60 min.

As shown, irradiation induced significant variations in the absorption spectra of both complexes. These changes appear to involve the entire spectral profile, including the $^1\pi\pi^*$ transitions of the ligands and the ^{1}MLCT regions, however, a progressive increase in a nonspecific background absorption was also observed, hampering a detailed analysis of the spectral variations interesting the ^{1}MLCT bands. For this reason, parallel experiments were performed in acetonitrile solutions. The obtained results, reported in the Figure S12, were complemented with high-resolution mass spectrometry measurements collected at the final points of the irradiation experiments, in order to gain further insight into the nature of the possible photodegradation products.

As shown in Figure S12, a progressive blue shift in the MLCT absorption bands is observed for both complexes, accompanied by a concomitant increase in the band intensity. Notably, this effect is significantly more pronounced for **RuCOCl** than for **OsCOCl**, highlighting the higher photoreactivity of the former complex. Indeed, the absorbance increase at 475 nm for **RuCOCl** exceeds twice the initial absorbance at the longest irradiation time investigated (120 min), whereas for **OsCOCl** the increase at 520 nm is limited to 0.41 under the same conditions. On the other hand, for shorter irradiation times, up to 20 min, only small variations were observed for the two complexes.

The behaviour observed in the UV-Vis titrations is consistent with the occurrence of photoinduced processes ascribable to the photorelease of the CO ligand, which modifies the electronic structure of the metal center and increases the energy of the ^{1}MLCT transitions. Complementary HR-ESI MS analysis performed on acetonitrile solutions of **RuCOCl** and **OsCOCl** subjected to LED irradiation times of 120 min further confirm the photorelease of a CO ligand, as it can be noted by the appearance of the isotopic patterns of the mono positively charged decarbonylated species [**RuCOCl**-CO-PF_6]$^+$ and [**OsCOCl**-CO-PF_6]$^+$, respectively centered at 653.08332 and 743.13870 (*m/z* = 1) in Figure S12b and S12d.

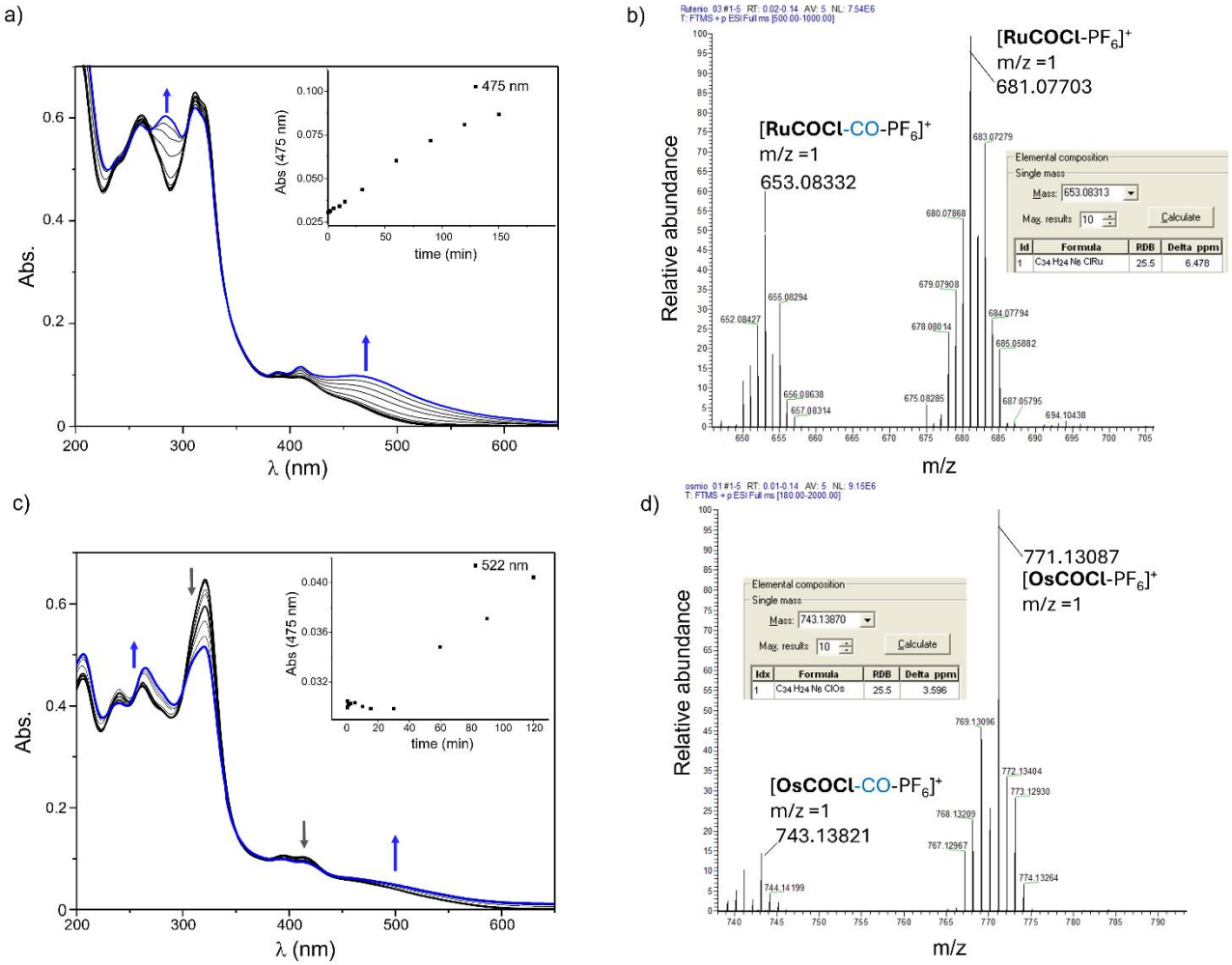

Figure S12: Photoreactivity of **RuCOCl** (a) and **OsCOCl** (c) investigated by UV-Vis spectroscopy and HR-ESI MS analysis (c, d). Acetonitrile solutions of the complexes (10 μM) were subjected to LED irradiation (160 mW) for increasing time intervals (0-120 min) and UV-Vis spectra were recorded. The final irradiated solutions were recovered and subjected to HR-ESI MS analysis (c,d).

Lastly, in order to evaluate the possible influence of CO-photorelease on the photosensitization properties and PDT performance of the two complexes, singlet oxygen quantum yields (ϕ_Δ) were determined for acetonitrile solutions of **RuCOCl** and **OsCOCl** previously subjected to 120 min of LED light irradiation, following the procedure already described in Section 2.

Our results indicated a marked decrease in the singlet oxygen sensitization efficiency of both complexes upon release or partial release of the CO ligand, with ϕ_Δ values decreasing from 0.60 ± 0.06 and 0.88 ± 0.06 for **RuCOCl** and **OsCOCl** to 0.26 ± 0.06 and 0.34 ± 0.06 for **RuCOCl** and **OsCOCl** preliminary photoactivated with 120 min LED irradiation.

Therefore, taken together, these findings highlight an additional and noteworthy aspect of the complexes investigated in this study, namely their ability to undergo photoinduced CO release, especially for **RuCOCl**.

It should be noted that these experiments were conducted in acetonitrile under prolonged irradiation conditions, which likely overestimate the extent of CO release and the associated decrease in singlet oxygen quantum yields. Under physiological (aqueous) conditions, where irradiation times are shorter and solvent effects differ, this behaviour is expected to be less pronounced without significantly altering the conclusions of the photodynamic therapy studies.

Nevertheless, this may open new perspectives for therapeutic applications beyond the role of **RuCOCl** and **OsCOCl** as PDT photosensitizers, such as in the context of photoCORMs-related activity, an important aspect which will be the subject of future investigations.

5. DFT calculations

5.1 Precursors

DFT calculations were performed to investigate the photophysical properties of Ru and Os precursors, **2a** and **2b** complexes. The performance of several exchange-correlation functionals were evaluated and the B3PW91 functional was selected for the complete characterisation of the precursors (Table S2). The main data describing the absorption spectra of **2a** and **2b** metal complexes are collected in Table S3 and Table S4. After the computational investigation of the photophysical properties of the precursors, relaxed scan calculations were carried out to determine the energy barriers associated with the reactions leading to the release of one of the CO ligands in both dark and light-irradiated conditions. Indeed, energy barriers were calculated starting from both **2a** and **2b** complexes in their ground state and from the triplet metal-to-ligand charge transfer (^{3}MLCT) state to the triplet dissociative metal-centered (^{3}MC) state. The corresponding potential energy scans, reported in Figure S13, were obtained by varying the metal-CO bond distance, starting from the geometry of the initial complexes.

In both cases, when the metal complexes are not irradiated, the CO ligand dissociation is very difficult to take place. For the Ru complex, CO detachment requires 39.9 kcal·mol^{-1}, whereas for the Os complex the required energy is approximately 10 kcal mol^{-1} higher. This analysis confirms that both complexes are stable in their ground states.

Upon photoexcitation, an abrupt transition from the ^{3}MLCT to the ^{3}MC state occurs with an activation energy barrier of 2.1 kcal·mol^{-1} along the reaction path for Ru and 17.0 kcal·mol^{-1} for Os. These results highlight the distinct reactivity of the two metals. In particular, the Ru complex, when irradiated, undergoes CO release to form a dissociative MC state stabilized by approximately 12 kcal mol^{-1} relative to the MLCT state, while the Os MC state formation is predicted to be endothermic by about 5 kcal mol^{-1}. Therefore, CO release is both kinetically and thermodynamically favoured in the ruthenium complex, whereas it is disfavoured in the osmium analogue. This difference can be rationalized by examining the electronic structure of the ground state of the two complexes. The Natural Bond Orbital (NBO) analysis was performed to investigate metal–ligand interactions, with particular emphasis on the metal-to-ligand back-donation toward the CO ligand. The LP(M) → π*(CO) second order interaction (where M = Ru or Os) describes the metal to ligand backdonation. The NBO results indicate that the LP(Ru) → π*(CO) interaction exhibits a stronger interaction compared to the LP(Os) → π*(CO) for the osmium complex. In particular, the stabilization energy (E^2) is 13.6 kcal mol^{-1} for **2a** and 22.5 kcal mol^{-1} for **2b** and this reduced back-donation correlates with a more favourable CO release, consistent with computational outcomes.

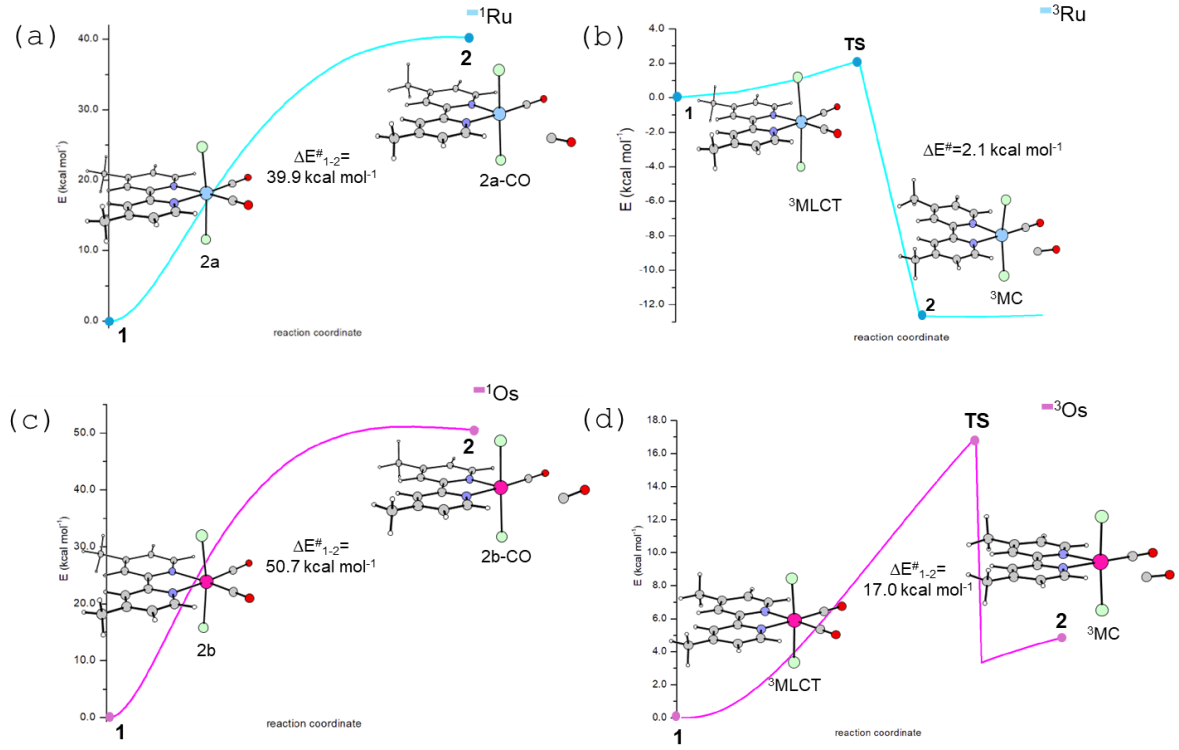

Figure S13. Relaxed potential energy scans from (a) **2a** Ru and (c) **2b** Os complexes, and from the ^{3}MLCT to ^{3}MC states for (b) Ru and (d) Os complexes, obtained by varying the distance between the metal center and the CO ligand.

Table S2 : TD-DFT benchmark for the reproduction of the experimental spectrum of the **$Os(CO)_2Cl_2$** in acetonitrile implicit solvent

Fuctional	State	ΔE	λ	f	Exp
B3LYP	S1	3.09	401	0.0012	436
	S2	3.24	382	0.0394	378
B97D	S1	2.34	530	0.0011	
	S2	2.48	500	0.0242	
B3PW91	S1	3.02	410	0.0014	
	S2	3.19	388	388.61	
CAM-B3LYP	S1	3.76	330	0.0000	
	S2	3.88	319	0.0053	
PBE	S1	2.20	562	0.0013	
	S2	2.37	522	0.0256	
PBE0	S1	3.20	387	0.0013	
	S2	3.37	368	0.0418	
M05	S1	3.33	372	0.0006	
	S2	3.48	356	0.0338	
M06	S1	3.22	385	0.0010	
	S2	3.37	367	0.0369	
M06L	S1	266	467	0.0110	
	S2	280	442	0.0251	
MN15	S1	3.52	352	0.0000	
	S2	3.55	349	0.0014	
M052X	S1	3.61	343	0.0000	
	S2	3.72	332	0.0072	
MN15L	S1	2.89	429	0.0014	
	S2	3.07	404	0.0355	
MN12L	S1	2.88	429	0.0014	
	S2	3.07	404	0.0403	

Table S3: Regions with theoretical assignments, excitation energies ΔE (eV), absorption wavelength λ (nm), oscillator strength f and MO contribution % for selected transitions Tr of **$Ru(CO)_2Cl_2$** complex calculated by B3PW91 functional, in acetonitrile solution.

Tr[a]	Region (Theoretical Assignment)	ΔE	λ	f	MO contribution[b]
Tr1	I(MLCT)	3.26	381	0.0002	H→L (100%)
Tr2		3.38	367	0.0258	H-1→L (99%)
Tr3	II(MLCT)	4.27	290	0.1249	H-2→L (49%), H→L+2 (46%)
Tr4		4.39	283	0.2404	H-2→L (41%), H→L+2 (51%)
Tr5		4.61	269	0.0607	H-1→L+3 (93%)
Tr6		4.76	260	0.0964	H-5→L (82%)
Tr7		4.85	255	0.0003	H-6→L (82%)
Tr8	III(LC/LLCT)	5.40	230	0.1229	H-2→L+2 (63%)
Tr9		5.48	226	0.1150	H→L+7 (29%), H-2→L+3 (24%)
Tr10		5.50	225	0.0908	H-2→L+3 (16%), H→L+7 (54%)
Tr11		6.04	205	0.0762	H-11→L (64%)
Tr12		6.10	203	0.5261	H-5→L+3 (52%), H-6→L+2 (27%)
Tr13		6.18	201	0.0404	H-7→L+5 (47%), H-1→L+10 (18%)

Tr = transition number. [a] Only vertical transitions with oscillator strength greater than 0.040 are reported, with the exception of the vertical transition in the 400-500 nm range with oscillator strength greater than 0.0001. [b] Only contributions larger than 15% are reported

Table S4: Regions with theoretical assignments, excitation energies ΔE (eV), absorption wavelength λ (nm), oscillator strength f and MO contribution % for selected transitions Tr of **$Os(CO)_2Cl_2$** complex calculated by B3PW91 functional, in acetonitrile solution.

Tr[a]	Region (Theoretical Assignment)	ΔE	λ	f	MO contribution
Tr1	I (MLCT)	3.02	410	0.0014	H→L (100%)
Tr2		3.19	389	0.0380	H-1→L (100%)
Tr3	II(MLCT)	4.29	289	0.0293	H→L+2 (65%), H-1→L+1 (33%)
Tr4		4.30	288	0.2438	H-2→L (64%), H-1→L+2 (22%)
Tr5		4.44	279	0.1916	H-1→L+2 (77%), H-2→LUMO (18%)
Tr6		4.78	259	0.1030	H-5→L (84%)
Tr7	III (LC/LLCT)	5.38	230	0.1381	H-2→L+1 (71%)
Tr8		5.44	228	0.1737	H-2→L+2 (45%), H-5→L+1 (11%)
Tr9		5.58	222	0.0543	H→L+6 (27%), H-6→L+3 (16%)
Tr10		5.93	209	0.0477	H-7→L+1 (74%)

Tr = transition number. [a] Only vertical transitions with oscillator strength greater than 0.040 are reported, with the exception of the vertical transition in the 400-500 nm range with oscillator strength greater than 0.0001. [b] Only contributions larger than 15% are reported

5.2 RuCOCl and OsCOCl complexes

DFT calculations were also carried out to investigate in depth the photophysical properties of Ru and Os complexes, along with their corresponding isomers. The performance of several exchange-correlation functionals were evaluated (Table S5), and the M05 meta-GGA exchange-correlation functional was selected for the complete characterisation of the metal complexes. The following discussion focuses on the synthesized Ru and Os complexes and obtained in the highest yield. Both calculated electronic spectra in water solution exhibit a long low-energy tail in the 400–500 nm region (I), originating from MLCT transitions, together with three additional absorption bands in the 200–400 nm range (II, III, and IV). These findings are consistent with the photophysical behaviour observed experimentally. The electronic transitions describing the absorption spectra of all the investigated systems, were fully characterized and are collected in Table S6-S9. In order to shed light on the photoactive potential of the explored systems, a detailed TDDFT analysis of their excited states was carried out. Efficient population of the triplet manifold via intersystem crossing (ISC) is crucial for this purpose. All the possible deactivation channels that involve the singlet states in the 400-500 nm region were taken into consideration. The excited state character, together with the MO contributions are described in Table S10 for Ru and Table S11 for Os. The feasibility of ISC from these singlet states to the triplet manifold was evaluated calculating spin–orbit coupling matrix elements and singlet–triplet energy gaps, as summarized in Table S12.

For both complexes, large spin–orbit coupling (SOC) values were obtained, with osmium exhibiting SOC values approximately one order of magnitude higher than the ruthenium complex. The introduction of a heavy atom into photosensitizing dyes is, in principle, expected to enhance SOC through the internal heavy atom effect. Therefore, the significantly higher SOC values observed for the Os complex are, very likely, a direct consequence of the fact that osmium is significantly heavier than ruthenium. In the case of the ruthenium complex, the strongest couplings occur between the S2 state, characterized by a charge-transfer (CT) contribution of 91.4% that is prominently (70%) of MLCT nature, and the triplet states T2 and T7, which display a similar MLCT character. The corresponding SOC values are 30.7 and 42.1 cm^{-1}, respectively. However, the smaller S2-T7 energy gap increases the population probability of the T7 triplet state respect to T2, enhancing the SOC value in accordance with El-Sayed's rules.[7] For the osmium complex, similar considerations valid for the ruthenium analogue can be extended. In particular, the largest SOC values are associated with states of similar nature, specifically those exhibiting MLCT character. The highest couplings, of 230.4, 277.5, and 264.7 cm^{-1}, are found for the S3–T3, S3–T7, S4–T7, and S4–T7 state pairs. The S4–T8 coupling, which displays an energy gap of 0.10 eV, also suggests a possible population of the T8 triplet state, although its lower SOC value may be attributed to the mixed (LC/MLCT) character of this triplet. The same investigation was conducted for the ruthenium and osmium isomers. The SOC values are high for both systems, exhibiting very similar behaviours. The data regarding the excited states involved in ISC processes are reported in Table S13 and S14, while the SOC values are listed in Table S15.

Table S5: TD-DFT benchmark for the reproduction of the experimental spectrum of the **RuCOCl** complex on the structure optimized at B3LYP-D3/6-31G** level in water implicit solvent. The tail of the experimental spectrum was also taken into consideration for the choice of the most suitable functional.

Fuctional	State	ΔE	λ	f
B3LYP	S1	2.89	428	0.0014
	S2	3.07	405	0.0355
O3LYP	S1	2.13	583	0.0137
	S2	2.21	561	0.0144
B97D	S1	1.51	819	0.0052
	S2	1.95	634	0.0029
B3PW91	S1	2.35	528	0.0000
	S2	2.57	481	0.0310
CAM-B3LYP	S1	2.85	435	0.0386
	S2	3.24	382	0.0006
PBE	S1	1.35	918	0.0068
PBE0	S1	2.44	508	0.0211
	S2	2.84	437	0.0533
M05	S1	2.39	518	0.0022
	S2	2.65	467	0.0519
M05+optM05	S1	2.41	515	0.0223
	S2	2.71	458	0.0495
M06L	S1	1.71	723	0.0065
MN15	S1	2.62	472	0.0003
	S2	2.66	465	0.0295
M052X	S1	2.83	438	0.0003
M062X	S1	2.67	464	0.0002
MN12L	S1	2.19	566	0.0152
	S2	2.29	494	0.0000

Table S6: Excitation energies ΔE (eV), absorption wavelength λ (nm), oscillator strength f and MO contribution % for selected transitions Tr of **RuCOCl** complex calculated by M05 functional, in water solution.

Tr	Region (Theoretical Assignment)	ΔE	λ	*f* [a]	MO contribution[b]
Tr1	I (MLCT)	2.41	515	0.0223	H→L (99%)
Tr2		2.71	457	0.0495	H-1→L (90%)
Tr3		3.09	401	0.0440	H-1→L+1 (52%), H-2→L (26%)
Tr4		3.11	399	0.0830	H-2→L (63%), H-1→L+1 (26%)
Tr5		3.30	376	0.0885	H-4→L (49%),H→L+3 (32%)
Tr6	II (MLCT/LC)	3.56	349	0.0493	H-1→L+3 (84%)
Tr7		3.68	336	0.0430	H-1→L+8 (48%)
Tr8		3.77	329	1.7016	H→L+3 (62%),H-4→L (28%)
Tr9		4.33	286	0.2245	H-6→L+2 (76%)
Tr10	III (LC/MLCT/LLCT)	4.64	267	0.1583	H-6→L+1 (78%)
Tr11		4.68	265	0.1002	H-1→L+11 (30%)
Tr12		4.72	263	0.1692	H-1→L+6 (23%)
Tr13		4.81	257	0.0791	H-8→L+1 (55%)
Tr14		4.83	256	0.0894	H-7→L+2 (46%)
Tr15		4.89	253	0.7626	H-7→L+3 (40%), H→L+9 (20%)
Tr16	IV(LLCT)	5.18	239	0.1349	H-3→L+5 (60%)
Tr17		5.90	210	0.1053	H→L+13 (29%)
Tr18		5.92	209	0.1684	H-6→L+5 (23%)

Tr = transition number. [a] Only vertical transitions with oscillator strength greater than 0.040 are reported, with the exception of the vertical transition in the 400-500 nm range with oscillator strength greater than 0.0001. b Only contributions larger than 15% are reported.

Table S7: Excitation energies ΔE (eV), absorption wavelength λ (nm), oscillator strength *f* and MO contribution % for selected transitions Tr of **OsCOCl** complex calculated by M05 functional, in water solution.

Tr[a]	Region (Theoretical Assignment)	ΔE	λ	*f* [a]	MO contribution[b]
Tr1	I (MLCT)	2.40	516	0.0226	H-1→L (98%)
Tr2		2.41	515	0.0530	H→L (92%)
Tr3		2.81	442	0.0626	H→L+1 (27%), H→L+2 (61%)
Tr4		2.97	418	0.0351	H-2→L (89%)
Tr5		3.29	377	0.0675	H-4→L (57%), H-1→L+3 (34%)
Tr6		3.32	373	0.0868	H-2→L+2 (60%), H→L+3 (18%)
Tr7	II (LC/MLCT)	3.77	329	1.2676	H-4→L (29%), H-1→L+3 (51%)
Tr8		4.25	292	0.0582	H-6→L+1 (20%)
Tr9		4.27	290	0.0671	H-3→L+3 (35%)
Tr10	III (MLCT/LLCT/LC)	4.47	277	0.0574	H-2→L+4 (48%)
Tr11		4.61	269	0.1792	H-2→L+5 (70%)
Tr12		4.63	268	0.0979	H-1→L+4 (47%)
Tr13		4.64	267	0.0589	H-1→L+4 (27%)
Tr14		4.66	266	0.0652	H→L+13 (34%)
Tr15		4.68	265	0.1215	H-4→L+3 (15%)
Tr16		4.71	263	0.1674	H-11→L (22%), H-1→L+7 (28%)
Tr17		4.77	260	0.0535	H-7→L+1 (66%), H-7→L+2 (19%)
Tr18		4.84	256	0.1146	H-3→L+4 (60%)
Tr19		4.86	255	0.14	H-9→L+2 (47%)
Tr20		4.89	253	0.7222	H-7→L+3 (31%), H-1→L+7 (21%)
Tr21		5.03	247	0.0708	H-3→L+5 (27%), H-3→L+8 (19%)
Tr22	IV (LC)	5.44	228	0.1524	H-10→L+2 (15%)
Tr23		5.47	225	0.0574	H-17→L (21%)
Tr24		5.51	210	0.1136	H-1→L+12 (18%)
Tr25		5.90	516	0.0226	H-1→L (98%)

Tr = transition number. a Only vertical transitions with oscillator strength greater than 0.040 are reported, with the exception of the vertical transition in the 400-500 nm range with oscillator strength greater than 0.0001. b Only contributions larger than 15% are reported.

Table S8: Excitation energies ΔE (eV), absorption wavelength λ (nm), oscillator strength f and MO contribution % for selected transitions Tr of **RuCOCl** isomer complex calculated by M05 functional, in water solution.

Tr	Region (Theoretical Assignment)	ΔE	λ	f[a]	MO contribution [b]
Tr1	I	2.39	518	0.0223	H→L (99%)
Tr2		3.06	405	0.1101	H-2→L (83%)
Tr3		3.14	395	0.0477	H-1→L+2 (93%)
Tr4		3.26	380	0.0699	H-3→L (42%), H→L+3 (21%)
Tr5	II	3.53	351	0.1808	H-4→L (14%), H-2→L+2 (53%)
Tr6		3.56	348	0.0915	H-4→L (21%), H-2→L+2 (41%)
Tr7		3.78	328	1.2885	H-4→L (28%), H→L+3 (48%)
Tr8		3.87	321	0.1505	H-7→L (33%), H-2→L+3 (22%)
Tr9		3.88	320	0.0481	H-7→L (46%), H-3→L+1 (30%)
Tr10		3.96	313	0.0407	H-2→L+3 (47%)
Tr11		4.00	310	0.0045	H-4→L+2 (23%), H-3→L+2 (42%)
Tr12	III	4.29	289	0.0467	H-6→L+2 (20%), H-1→L+6 (47%)
Tr13		4.55	272	0.0550	H-7→L+1 (28%), H-10→L (24%)
Tr14		4.63	268	0.0478	H-2→L+4 (77%)
Tr15		4.65	267	0.1145	H-1→L+11 (41%)
Tr16		4.69	264	0.1655	H→L+8 (16%), H→L+9 (16%)
Tr17		4.71	263	0.0886	H-4→L+2 (22%)
Tr18		4.77	260	0.0734	H-8→L+2 (18%), H-2→L+6 (54%)
Tr19		4.86	255	0.0893	H-9→L+1 (64%)
Tr20		4.92	252	0.0477	H-6→L+3 (83%)
Tr21		5.41	229	0.0857	H-18→L (22%), H-16→L (13%)
Tr22	IV	5.42	229	0.0971	H-15→L (17%), H-14→L (15%)
Tr23		5.88	211	0.0843	H-15→L+1 (11%), H→L+12 (37%)
Tr24		5.91	210	0.0998	H-9→L+4 (35%)
Tr25		5.94	209	0.0480	H→L+13 (19%)
Tr26		6.01	206	0.1107	H-15→L+2 (15%), H-6→L+6 (16%)

Tr = transition number. a Only vertical transitions with oscillator strength greater than 0.040 are reported, with the exception of the vertical transition in the 400-500 nm range with oscillator strength greater than 0.0001. b Only contributions larger than 15% are reported.

Table S9: Excitation energies ΔE (eV), absorption wavelength λ (nm), oscillator strength *f* and MO contribution % for selected transitions Tr of **OsCOCl** isomer complex calculated by M05 functional, in water solution.

Tr[a]	Region (Theoretical Assignment)	ΔE	λ	*f*	MO contribution
Tr1		2.34	530	0.0004	H→L (75%), H→L+1 (24%)
Tr2		2.91	426	0.0460	H-2→L (85%)
Tr3		3.20	387	0.0659	H-3→L (39%), H-2→L+1 (26%)
Tr4		3.22	386	0.0479	H-1→L+1 (78%)
Tr5		3.27	380	0.0713	H-2→L+1 (54%), H-1→L+1 (12%)
Tr6		3.35	370	0.0428	H-2→L+2 (88%)
Tr7		3.42	363	0.0625	H-4→L (32%), H-3→L (25%)
Tr8		3.63	341	0.0445	H-1→L+2 (96%)
Tr9		3.76	330	1.1248	H-4→L (29%), H-1→L+3 (28%)
Tr10		3.77	329	0.5332	H-3→L+2 (48%), H-1→L+3 (18%)
Tr11		4.36	285	0.2416	H-6→L+2 (50%), H→L+5 (16%)
Tr12		4.39	283	0.1472	H-6→L+2 (24%), H→L+5 (45%)
Tr13		4.61	269	0.1434	H-4→L+2 (24%)
Tr14		4.62	268	0.1158	H→L+13 (29%)
Tr15		4.67	266	0.1841	H-4→L+2 (15%), H-2→L+6 (40%)
Tr16		4.68	265	0.1912	H-12→L (14%), H-1→L+7 (37%)
Tr17		4.80	258	0.0791	H-8→L+2 (71%)
Tr18		4.85	256	0.4552	H-7→L+3 (27%)
Tr19		4.89	254	0.1226	H-9→L+1 (36%), H-1→L+6 (20%)
Tr20		4.94	251	0.0414	H-7→L+2 (37%)
Tr21		4.97	249	0.0071	H-3→L+4 (27%), H→L+14 (15%)
Tr22		5.35	232	0.0758	H-9→L+3 (60%)
Tr23		5.43	228	0.1248	H-9→L+3 (15%), H-4→L+5 (15%)
Tr24		5.58	222	0.0418	H-18→L (40%)
Tr25		5.63	220	0.0756	H-11→L+2 (21%)
Tr26		5.67	219	0.0437	H-19→L (17%), H-13→L+1 (31%)
Tr27		5.88	211	0.0674	H-15→L+1 (19%), H-14→L+1 (40%)
Tr28		5.90	210	0.0593	H-4→L+5 (20%), H-4→L+6 (25%)
Tr29		5.95	208	0.0703	H-21→L+2 (15%), H-15→L+2 (15%)
Tr30		5.98	207	0.1535	H-9→L+4 (41%), H-8→L+4 (34%)
Tr31		6.02	206	0.0609	H-21→L+2 (17%), H-5→L+6 (15%)
Tr32		6.06	205	0.0418	H-4→L+7 (22%), H-16→L+3 (19%)
Tr33		6.11	203	0.1121	H-8→L+6 (30%), H-19→L+1 (10%),

Tr = transition number. [a] Only vertical transitions with oscillator strength greater than 0.040 are reported, with the exception of the vertical transition in the 400-500 nm range with oscillator strength greater than 0.0001. b Only contributions larger than 15% are reported.

Table S10: M05 excitation energies ΔE(eV), absorption wavelength λ (nm), oscillator strength f , charge transfer CT (%), MO contribution (%) and theoretical assignment for the singlet states and the triplet states of the RuCOCl complex involved in the ISC process

Singlet states						
States	ΔE	λ	f	CT	MO contributions [b]	Theoretical Assignment
S1	2.41	515	0.0223	0.2	H→L(99%)	LC (99.8%)
S2	2.71	458	0.0495	91.4	H-1→L(90%)	MLCT (70.1%)
Triplet states						
T1	0.87	1429	0.0000	0.2	H→L(94%)	LC(99.8%)
T2	2.32	534	0.0000	40.6	H-1→L+7(89%)	MC (57.2%%)/ MLCT(28.2%)
T3	2.42	513	0.0000	17.8	H-7→L(27%),H-1→L+1 (17%)	LC (81.2%)
T4	2.54	488	0.0000	18.1	H-4→L (45%), H-1→L (25%)	LC (81.8)
T5	2.58	480	0.0000	0.2	H-5→L (88%)	LC (99.8%)
T6	2.60	476	0.0000	8.8	H-6→L+2 (45%),	LC (90.8%)
T7	2.69	460	0.0000	62.8	H-1→L (36%), H-1→L+1 (26%)	MLCT (42.6%)

Table S11: M05 excitation energies ΔE(eV), absorption wavelength λ (nm), oscillator strength f , charge transfer CT (%), MO contribution (%) and theoretical assignment for the singlet states and the triplet states of the **OsCOCl** complex involved in the ISC process

Singlet states						
States	ΔE	λ	f	CT	MO contributions [b]	Theoretical Assignment
S1	2.40	516	0.0226	0.7	H-1→L (98%)	LC (99.3%)
S2	2.41	514	0.0530	89.6	H→L (92%)	MLCT (71.1%)
S3	2.65	468	0.0002	93.6	H→L+1 (69%)	MLCT (73.6%)
S4	2.81	442	0.0626	90.0	H→L+2 (61%), H→L+1 (27%)	MLCT (70.1%)
Triplet states						
T1	0.86	1434	0.0000	0.2	H-1→L (93%)	LC (99.8%)
T2	2.22	557	0.0000	60.2	H→L+2 (40%),H→L (20%)	MLCT (49.6%) / LC (37.9%)
T3	2.37	523	0.0000	60.3	H→L (65%)	MLCT (48.7%)/LC(39.5%)
T4	2.55	485	0.0000	26.0	H-7→L (22%), H→L+2 (22%)	LC (73.4%)
T5	2.56	486	0.0000	17.5	H-6→L+1 (31%), H-2→L+1 (11%)	LC (82.1%)
T6	2.58	480	0.0000	0.3	H-5→L(91%)	LC (99.7%)
T7	2.61	475	0.0000	79.4	H→L+1 (67%)	MLCT (62.2%)/ LC (17%)
T8	2.71	458	0.0000	29.1	H-4→L (59%)	LC(70.6%)/MLCT(22.1%)

Table S12. Spin orbit coupling constants (SOC, cm^{-1}) between the most important singlet states and triplet states lying below, together with their adiabatic energy difference (ΔE, eV) in parentheses, calculated for the **RuCOCl** and **OsCOCl** complexes.

$S_n \rightarrow T_m$	Sn	Tm							
		1	2	3	4	5	6	7	8
RuCOCl	1		1.46 (0.09)						
	2		30.7 (0.39)	21.8 (0.29)	25.4 (0.17)	12.0 (0.12)	3.2 (0.10)	42.1 (0.01)	
OsCOCl	1		39.1 (0.18)	36.9 (0.03)					
	2		2.2 (0.19)	6.5 (0.04)					
	3			159.0 (0.28)	5.1 (0.09)	59.7 (0.09)	85.3 (0.07)	230.4 (0.04)	
	4			277.5 (0.43)	44.7 (0.25)	13.4 (0.25)	73.5 (0.22)	264.7 (0.20)	145.5 (0.10)

Table S13: M05 excitation energies ΔE(eV), absorption wavelength λ (nm), oscillator strength f , charge transfer CT (%), MO contribution (%) and theoretical assignment for the singlet states and the triplet states of **the isomer** of the **RuCOCl (trans-Cl)** complex involved in the ISC process

Singlet states						
S States	ΔE	λ	f	CT	MO contributions [b]	Theoretical Assignment
S1	2.39	518	0.0223	0.2	H→L (99%)	LC (99.8%)
S2	2.66	466	0.0000	94.3	H-1→L (77%), H-1→L+1 (20%)	MLCT(72.2%)
S3	2.71	457	0.0001	44.2	H-1→L+7 (82%)	MC(56.2%)
S4	2.93	424	0.0002	53.0	H-5→L (40%), H-1→L+1 (47%)	LC(44.7%)
S5	2.96	419	0.0013	41.2	H-5→L (56%), H-1→L (12%), H-1→L+1 (28%)	LC(57.4%)
S6	3.06	405	0.1101	82.6	H-2→L (83%)	MLCT(49.5%)
Triplet states						
T1	0.86	1437	0.0000	0.2	H→L (93%), H→L+5 (11%)	LC (99.8%)
T2	2.27	547	0.0000	40.6	H-1→L+7 (83%)	MCLT(28%)
T3	2.45	507	0.0000	7.2	H-7→L (34%), H→L+5 (11%)	LC(92.6%)
T4	2.56	484	0.0000	22.6	H-6→L+2 (36%), H-1→L+2 (21%)	LC(75.7%)
T5	2.57	482	0.0000	14.5	H-5→L (67%), H-1→L (12%)	LC(84.8%)
T6	2.57	482	0.0000	4.3	H-4→L (24%), H-3→L (46%)	LC(95.6%)
T7	2.62	472	0.0000	66.3	H-5→L (18%), H-1→L (33%), H-1→L+1 (30%)	MLCT(50.7%)
T8	2.80	443	0.0000	72.4	H-1→L (45%), H-1→L+1 (12%), H-1→L+8 (16%), H-1→L+9 (14%)	MLCT(53.6%)
T9	2.90	428	0.0000	20.1	H-10→L (14%), H-2→L+1 (17%), H→L+5 (12%), H→L+10 (10%)	LC(79.2%)
T10	2.96	419	0.0000	15.3	H-3→L+1 (11%), H→L+3 (24%)	LC(83.6%)
T11	2.98	416	0.0000	55.2	H-6→L+2 (12%), H-2→L+7 (10%), H-1→L+2 (47%)	MLCT (41.9%), LC(37.0%)
T12	2.99	415	0.0000	51.4	H-2→L+7 (65%)	MLCT(22.6%)
T13	3.05	406	0.0000	73.7	H-1→L+1 (47%), H-1→L+8 (18%), H-1→L+9 (16%)	MLCT(55.6%)

Table S14: M05 excitation energies ΔE(eV), absorption wavelength λ (nm), oscillator strength f , charge transfer CT (%), MO contribution (%) and theoretical assignment for the singlet states and the triplet states of **the isomer** of the **OsCOCl** complex **(trans-Cl)** involved in the ISC process

Singlet states						
States	ΔE	λ	f	CT	MO contributions [b]	Theoretical Assignment
S1	2.34	530	0.0004	95.1	H→L (75%), H→L+1 (24%)	MLCT (73.8%)
S2	2.39	520	0.0222	0.2	H-1→L (99%)	LC (99.8%)
S3	2.62	473	0	93.8	H→L+1 (74%), H→L (24%)	MLCT (72.6%)
S4	2.81	441	0.1088	89.4	H→L+2 (94%)	MLCT(70.1%)
Triplet states						
T1	0.86	1444	0	0.2	H-1→L (93%), H-1→L+5 (12%)	LC (99.8%)
T2	2.32	535	0	92	H→L (65%), H→L+1 (30%)	MLCT (71.8%)
T3	2.38	522	0	53.4	H→L+2 (63%), H-6→L+2 (16%)	LC(45.0%), MLCT(44.0%)
T4	2.42	512	0	13	H-7→L (31%)	LC(86.8%)
T5	2.55	486	0	21.6	H-4→L (29%), H-3→L (18%)	LC(77.8%)
T6	2.57	483	0	26.4	H-5→L (43%), H→L+1 (21%)	LC(72.7%)
T7	2.61	474	0	52.9	H-5→L (40%), H→L+1 (32%)	LC(45.7%), MLCT(40.5%)
T8	2.78	446	0	32.8	H-6→L+2 (38%), H→L+2 (24%)	LC(66.3%), MLCT(24.2%)

Table S15: Spin orbit coupling constants (SOC, cm^{-1}) between the most important singlet states and triplet states lying below, together with their adiabatic energy difference (ΔE, eV) in parentheses, calculated for the isomer of **RuCOCl(trans-Cl)** , **OsCOCl (trans-Cl)** complexes.

$S_n \rightarrow T_m$	Sn	Tm												
		1	2	3	4	5	6	7	8	9	10	11	12	
RuCOCl (trans-Cl)	1		1.4 (0.13)											
	2		30.6 (0.39)	22.1 (0.21)	25.8 (0.10)	11.7 (0.09)	3.2 (0.08)	41.8 (0.03)						
	3		7.3 (0.44)	7.8 (0.26)	91.6 (0.15)	11.4 (0.14)	19.3 (0.14)	94.3 (0.09)						
	4			14.3 (0.48)	7.7 (0.36)	0.6 (0.35)	15.4 (0.35)	1.5 (0.30)	0.4 (0.13)	0.3 (0.03)				
	5			(0.51)	39.1 (0.40)	4.3 (0.39)	39.0 (0.39)	45.2 (0.34)	102.1 (0.16)	56.0 (0.06)	30.6 (0.01)			
	6			(0.61)	119.1 (0.50)	14.3 (0.49)	137.0 (0.49)	11.8 (0.44)	65.8 (0.26)	17.4 (0.16)	38.5 (0.10)	24.9 (0.08)	42.0 (0.07)	
OsCOCl (trans-Cl)	1		11.5 (0.02)											
	2		9.6 (0.07)	3.8 (0.01)										
	3		35.6 (0.30)	16.1 (0.24)	86.2 (0.20)	97.5 (0.07)	48.8 (0.05)	117.5 (0.01)						
	4			99.9 (0.43)	125.4 (0.39)	71.6 (0.26)	129.9 (0.24)	143.2 (0.20)	43.9 (0.03)					

5.3 Computational details

All molecular geometry optimizations of the ground and excited states of the investigated metal complexes were performed using the Gaussian 16 software package.[8] The B3PW91 functional[9] was employed for the precursor species, while the M05 functional[10] was used for the final complexes. The standard 6–31G(d,p) basis set was applied to all atoms except for Ru and Os, for which the SDD effective core potential and the corresponding valence basis set[11] were adopted. All calculations for the precursor complexes were carried out in acetonitrile solvent, whereas those for the final complexes were conducted in water, in order to better reproduce physiological conditions. The photophysical properties and optical absorption spectra of the investigated systems were simulated using time-dependent density functional theory (TDDFT) based on the optimized ground-state geometries. To properly characterize the nature of the electronic transitions, fragment-based analyses were carried out using the TheoDORE (Theoretical Density, Orbital Relaxation, and Exciton Analysis) program.[12] The ORCA 5.0.4 package[11] was employed to explore the intersystem crossing (ISC) mechanisms between the selected singlet and triplet excited states at the ground-state geometry. Relativistic effects were accounted for using the zeroth-order regular approximation (ZORA) in combination with the M05 functional. The ZORA-DEF2-SVP and old-ZORA-SVP basis sets were used for all atoms and for the metal centers, respectively, consistent with our previous studies on ruthenium and osmium complexes.[14-16] The RIJCOSX approximation was applied to accelerate the computations, as recommended in the ORCA manual. The spin–orbit coupling (SOC) values were calculated as the square root of the sum of the squared moduli of the corresponding matrix elements:

$$SOC_{mn} = \sqrt{\sum_i \left|\left\langle \Psi_{S_m} \middle| \widehat{H_{SO}} \middle| \Psi_{iT_n} \right\rangle\right|};\ i = x,y,z$$

6. Biological studies

6.1 Cell culture and treatments

Human A431 cells (ATCC® CRL-1555™) were routinely cultured in Dulbecco's modified Eagle's medium (DMEM) supplemented with 10% fetal bovine serum (FBS), 2 mM L-glutamine, 100 U/mL penicillin, and 100 µg/mL streptomycin, at 37 °C in a humidified 5% CO_2 atmosphere.

For treatments, the medium was replaced with serum-free DMEM, and cells were exposed to increasing concentrations (0, 0.001, 0.01, 0.1, 1, and 10 µM) of **RuCOCl** or **OsCOCl** for 1 h.

6.2 Cellular uptake

Cells were seeded on sterile glass coverslips in 6-well plates (approximately 4 × 10^5 cells/well) in DMEM supplemented with 10% FBS and grown for 24 h until reaching confluence. After 1 h treatment with Ru(II) and Os(II) complexes, cells were washed twice with PBS and fixed with 3% paraformaldehyde. Permeabilization and quenching were performed for 30 min at room temperature using 0.1% Triton X-100 and ethanolamine (1:165) in PBS. Nuclei were stained with DAPI (#MBD0015, Sigma-Aldrich, MA, USA) for 30 min in the dark. Coverslips were then mounted using Fluoromount Aqueous Mounting Medium (Sigma-Aldrich, MA, USA), and fluorescence images were acquired on a Leica SP8 laser scanning confocal microscope (Leica Microsystems GmbH, Wetzlar, Germany) equipped with a 63× oil-immersion objective.

The intrinsic fluorescent properties of **RuCOCl** and **OsCOCl** enabled monitoring of internalization kinetics but did not allow quantitative estimation due to their different emissive efficiencies. To overcome this limitation, cellular uptake of the Ru(II) and Os(II) complexes in A431 cells was quantified by measuring intracellular ruthenium and osmium content in cell lysates using Inductively Coupled Plasma Mass Spectrometry (ICP-MS) after 3 h incubation at 1 and 10 µM (Figure S14). As shown, the metal internalization was particularly evident at 10 µM, reaching approximately 200 ng of Ru and 450 ng of Os per 10^6 cells after 3 h incubation.

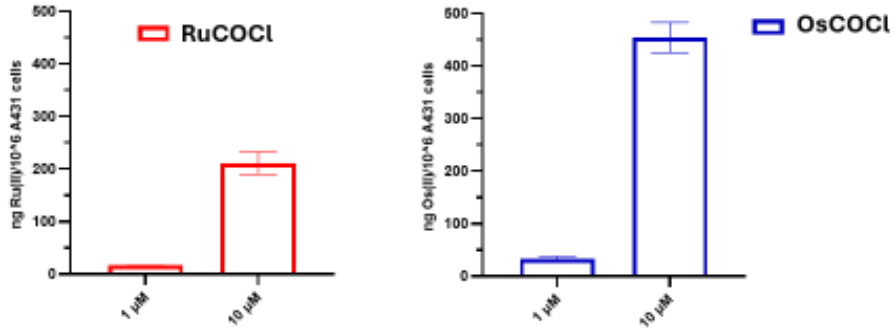

Figure S14: Quantification of intracellular metal content by ICP-MS. ICP-MS analysis was performed in A431 cells incubated with 1-10 µM **RuCOCl** and **OsCOCl** for 3 hours to determine the intracellular concentration of Ru and Os, expressed as ng metal per 10^6 cells. All data represent mean ± SEM of n = 3 independent experiments.

6.3 Cell viability assay

Cellular viability was assessed by MTT reduction assay. Approximately 2×10^4 A431 cells per well were seeded in two 96-well plates. Once confluence was reached, cells were treated with **RuCOCl** or **OsCOCl** at different concentrations (0, 0.001, 0.01, 0.1, 1, and 10 µM) in serum-free DMEM supplemented with 0.1% BSA. All conditions were performed in hexaplicate. After 1 h of incubation, one plate was subjected to irradiation for 15 min, while the other was maintained in the dark. After 24 h, the culture medium was removed, and cells were washed once with sterile, antibiotic-free PBS. Then, 200 µL per well of 1 × MTT solution was added, and plates were incubated for 30 min in the dark. After incubation, the MTT solution was aspirated, and 150 µL per well of 100% DMSO was added to lyse the cells and solubilize the formazan crystals. Absorbance was measured at 595 nm using VICTOR Nivo Multimode Microplate Reader (Revvity).

REFERENCES

1 C. Bischof, T. Joshi, A. Dimri, L. Spiccia and U. Schatzschneider, *Inorg. Chem.*, , DOI:10.1021/ic400746n.

2 C. M. Kepert, G. B. Deacon, N. Sahely, L. Spiccia, G. D. Fallon, B. W. Skelton, A. H. White, *Inorg. Chem.*, 2004, 43, 2818-2827, DOI 10.1021/ic0351895

3 G. Sambucari, C. Coutant, A. Di Michele, G. E. Giacomazzo, P. Nun, V. Sol, N. Renard, T. Ouk, V. Coeffard and M. Di Donato, *Adv. Opt. Mater.*, 2025, **13**, 1–11.

4 G. E. Giacomazzo, S. Doria, A. Revilla-Cuesta, N. De Monte, M. Pagliai, G. Pietraperzia, B. Valtancoli, T. Torroba, L. Conti, M. Di Donato and C. Giorgi, *Inorg. Chem.*, 2024, **63**, 6248–6259.

5 L. Conti, A. Bencini, C. Ferrante, C. Gellini, P. Paoli, M. Parri, G. Pietraperzia, B. Valtancoli and C. Giorgi, *Chem. – A Eur. J.*, 2019, **25**, 10606–10615.

6 M. Montalti, A. Credi, L. Prodi, M. T. Gandolfi, HANDBOOK OF PHOTOCHEMISTRY, 10.1201/9781420015195.

7 M. A. El-Sayed, Spin—orbit coupling and the radiationless processes in nitrogen heterocyclics, J. Chem. Phys., 1963, 38, 2834–2838.

8 Gaussian 16, Revision B.01, Frisch, M.J., Trucks, G.W., Schlegel, H.B., Scuseria, G.E., Robb, M.A., Cheeseman, J.R.; Scalmani, G.; Barone, V.; Petersson, G.A.; Nakatsuji, H.; Li, X.; Caricato, M.; Marenich, A.V.; Bloino, J., Janesko, B.G., Gomperts, R., Mennucci, B., Hratchian, H.P., Ortiz, J.V., Izmaylov, A.F., Sonnenberg, J.L., Williams-Young, D., Ding, F., Lipparini, F., Egidi, F., Goings, J., Peng, B., Petrone, A., Henderson, T., Ranasinghe, D., Zakrzewski, V.G., Gao, J., Rega, N., Zheng, G., Liang, W., Hada, M., Ehara, M., Toyota, K., Fukuda, R., Hasegawa, J., Ishida, M., Nakajima, T., Honda, Y., Kitao, O., Nakai, H., Vreven, T., Throssell, K., Montgomery Jr., J.A., Peralta, J.E., Ogliaro, F., Bearpark, M.J., Heyd, J.J., Brothers, E.N., Kudin, K.N., Staroverov, V.N., Keith, T.A., Kobayashi, R., Normand, J., Raghavachari, K., Rendell, A.P., Burant, J.C., Iyengar, S.S., Tomasi, J., Cossi, M., Millam, J.M., Klene, M., Adamo, C., Cammi, R., Ochterski, J.W., Martin, R.L., Morokuma, K., Farkas, O., Foresman, J.B., Fox, D.J. Gaussian, Inc., Wallingford CT (2016) GaussView 5.0. Wallingford, E.U.A. - References - Scientific Research Publishing, https://www.scirp.org/reference/referencespapers?referenceid=2418053, (accessed October 23, 2025).

9 A. D. Becke, *The Journal of Chemical Physics*, 1993, **98**, 5648–5652.

10 Y. Zhao, N. E. Schultz and D. G. Truhlar, *J. Chem. Phys.*, 2005, **123**, 161103.

11 D. Andrae, U. Häußermann, M. Dolg, H. Stoll and H. Preuß, *Theoret. Chim. Acta*, 1990, **77**, 123–141.

12 F. Plasser, *J. Chem. Phys.*, 2020, **152**, 084108.

13 F. Neese, *WIREs Comput Mol Sci*, 2012, **2**, 73–78.

14 P. Barretta, F. Ponte and G. Mazzone, *Journal of Molecular Liquids*, 2024, **402**, 124761.

15 P. Barretta, F. Ponte, D. Escudero and G. Mazzone, *Molecules*, 2024, **29**, 4298.

16 D. Belletto, F. Ponte, G. Mazzone and E. Sicilia, *Dalton Trans.*, 2024, **53**, 8243–8253.